# STARS, STAR FORMATION, AND DARK MATTER CORES IN DWARF GALAXIES

# THE DYNAMICAL IMPLICATIONS FOR STARS, STAR FORMATION, AND DARK MATTER CORES IN DWARF GALAXIES

By

Aaron J. Maxwell, B.Sc. Honours, M.Sc.

A Thesis

Submitted to the School of Graduate Studies

in Partial Fulfillment of the Requirements

for the Degree of

Doctor of Philosophy

McMaster University

DOCTOR OF PHILOSOPHY (2014)
(Physics and Astronomy)

McMaster University
Hamilton, Ontario

TITLE: The Dynamical Implications for Stars, Star Formation, and Dark Matter Cores in Dwarf Galaxies

AUTHOR: Aaron Joshua Maxwell, B.Sc. Honours (York University), M.Sc. (University of Victoria)

SUPERVISORS: Dr. James Wadsley and Dr. Hugh Couchman

NUMBER OF PAGES: XIV, 113

# Abstract

I investigate the observational signatures of the formation of dark matter cores in dwarf galaxies. I adopt the paradigm where the energy from star formation feedback is injected into the orbits of dark matter particles, forming a constant density core consistent with observations of dwarf galaxies. Using physically motivated constraints I show there is ample feedback energy available given the average stellar mass of dwarf galaxies to form cores in $10^8$–$10^{11}\,M_\odot$ halos, and predict the maximum core size as a function of stellar mass. I describe how observational features of the old stellar content of dwarf galaxies are due to this core formation paradigm. As both dark matter and stars are collisionless fluids, the stars responsible for the feedback form in the centres of dwarf galaxies and have their orbits grown by subsequent star formation. This will naturally lead to age and metallicity gradients, with the younger and more metal rich stellar population near the dwarf centres. This process also prevents the destruction of globular clusters by driving them out of the dwarf nucleus — the decrease in central dark matter density reduces the strength of dynamical friction — and increases the likelihood of being stripped onto the stellar halos of larger galaxies. It also offers a model for forming multiple populations in globular clusters, with the only assumption being that the source of the polluted gas resides within the dwarf progenitor. As the orbit of a globular cluster grows, it will experience multiple accretion events with each pass through the gas-rich galaxy centre. The simple accretion model exhibits two traits revealed from observations — a short accretion timescale and a sensitive dependence on mass — without requiring an exotic initial stellar mass function or the initial globular cluster mass function to be 10–25 times larger than at present.

*For Rachel Louise,*
*My best friend and partner in crime*

# Co-Authorship

Chapters 2, 3, and 4 of this thesis contain original scientific research written by myself, Aaron Joshua Maxwell. Chapter 2 has been submitted to the peer-reviewed Astrophysical Journal. The reference to this work is:

*Maxwell, Aaron J., Wadsley, J. and Couchman, H. M. P., manuscript no. ApJ96454*

My co-supervisors, Dr. James Wadsley and Dr. Hugh Couchman, are the second and third authors.

Chapter 3 has been published as a peer-reviewed journal article in the Astrophysical Journal Letters (ApJL). The reference to this work is:

*Maxwell, Aaron J., Wadsley, J., Couchman, H. M. P., and Mashchenko, S., 2012, ApJ, Volume 755, Issue 2, pp. 35–39.*

Again, Dr. James Wadsley and Dr. Hugh Couchman are the second and third authors, respectively. Dr. Sergey Mashchenko originally ran the simulations which I have used extensively in my thesis, and provided a suite of codes that I modified for my analysis.

Chapter 4 has been published as a peer-reviewed journal article in the Monthly Notices of the Royal Astronomical Society (MNRAS). The reference to this work is:

*Maxwell, Aaron J., Wadsley, J., Couchman, H. M. P., and Sills, A., 2014, MNRAS, Volume 439, Issue 2, pp. 2043–2049.*

As before, Dr. James Wadsley and Dr. Hugh Couchman are the second and third authors, respectively. Dr. Alison Sills helped shape the ideas presented in this paper, and was indispensable for her knowledge in regards to multiple stellar populations in globular clusters.

All previously published material has been reformatted to conform to the required thesis style. I hereby grant an irrevocable, non-exclusive license to McMaster University and the National Library of Canada to reproduce this material as part of this thesis.

# Acknowledgements


Well, I'm glad that's over . . .

Achieving a doctorate, no matter the field, is a long and rigorous endeavour, and it cannot be done alone. I've travelled all over the world, biked hundreds of kilometres, and managed to convince a beautiful woman to marry me. And that was all easier than getting the doctorate. Well, maybe not the marrying part; I worked pretty hard to woo . . . ahem, I mean wear her down.

I want to thank James and Hugh for letting me work on this project. It wasn't easy at any point, but I'm grateful that they let me pursue what I wanted.

In the four years I was here, I had opportunities to collaborate with many wonderful people. Sergey, thanks for all those chats that taught me what it was to be a galactic dynamicist. Alison, thank you for having an idle chat with James one day that turned into one of the most interesting projects I ever tackled. Kristine and Rachel, you may never read this, but you let me put my name on Canada-France-Hawaii *and Hubble-freakin'-Space Telescope* proposals! A space-science nerd's wet dream.

The many friends I made along the way, both here and at the University of Victoria, deserve thanks. You are too many to name, but you saved me from a life of eating my lunch alone at my desk.

My parents. You are a God-send. Thank you for instilling in me passion, fire, and the will to achieve my goals.

Finally, my lovely, beautiful, courageous, intelligent, sexy, hilarious wife. I am nothing without you. You gave me the strength every day to climb out of bed. You never let me wallow in depression or self-pity. When it was dark, you were my light. I love you like nothing else on this Earth.

"A thousand doors, a thousand lies; rooms a thousand years wide"

---

*Room a Thousand Years Wide*

KIM THAYIL (1960-)

"Long time coming, it seemed to get me by. Long time coming, it seemed to satisfy."

---

*Fresh Tendrils*

CHRIS CORNELL (1964-)

"Shall I compare thee to a summers' day? Thou art more lovely and more temperate."

---

*Sonnet 18*

WILLIAM SHAKESPEARE (1564-1616)

"To boldly go where no man has gone before."

JAMES T. KIRK (2233-2371)

"Cake, and grief counseling, will be available at the conclusion of the test."

*Aperture Science Enrichment Centre Test Experience*
GLADOS (2010)

"Try not. Do. Or do not. There is no try."

*The Empire Strikes Back*
YODA (896 BBY-4 ABY)

# List of Figures

# List of Tables

# List of Acronyms

**SF** Star Formation

**SFR** Star Formation Rate (mass per unit time)

**SPH** Smoothed Particle Hydrodynamics

**GC** Globular Cluster

**pc** Parsec ($3.08 \times 10^{16}$ metres or 3.26 ly)

**ly** Light years, the distance a beam of light would travel in a year

$z$ Cosmological redshift

**LG** The Local Group of galaxies

**LGD** The Local Group dwarf galaxies

**DSPH** Dwarf spheroidal, a class of galaxies

**ISM** The Interstellar Medium

**IMF** The Initial Stellar Mass Function

**WMAP** The Wilkinson Microwave Anisotropy Probe

**CMB** The Cosmic Microwave Background

**POSS-II** Second Palomar Observatory Sky Survey

**CalTech** California Institute of Techonology

**AAO** Anglo-Australian Observatory

**ROE** Royal Observatory Edinburgh

**STScI** Space Telescope Science Institute

**R-band** A broad-band image filter centered at 650 nm i.e. red

Chapter 1

# Introduction

Only 5% of our universe is made up of matter currently described by the standard model of particle physics. The other 95% is split into two components: particles of matter that emit no measurable amount of light (hence, dark matter) that comprises 25% of the density of the universe, while the remaining 70% is labelled dark energy[1] (Planck Collaboration et al., 2014). Although we cannot directly detect its presence, dark matter has a significant influence on the formation of all luminous structures in the universe. All galaxies are thought to be seeded at the bottom of deep gravitational wells formed by surrounding halos of dark matter, significantly speeding up the process by which atomic and molecular gas was able to collapse to high enough densities to form stars. Thus, it is of fundamental importance that we understand the nature of dark matter.

Over the past four decades, our simple picture of dark matter — massive particles that interact only through gravity — has been seriously challenged. The numerical predictions of the number of dark matter halos and their inner density

[1] There currently exists no physical explanation of what dark energy is, but it is driving the accelerated expansion of our universe and was only recently verified (Riess et al., 1998; Perlmutter et al., 1999).

distributions differ substantially from what is inferred by observations. Resolving these discrepancies requires an understanding of the physical processes at work as a galaxy forms at the centre of a dark matter halo.

## 1.1 The Current Cosmological Model

Our universe is currently described by a cosmological model ($\Lambda$CDM) that best fits the Cosmic Microwave Background (CMB), shown in Figure 1.1. First discovered by Penzias & Wilson (1965), it is the relic thermal radiation left over from the formation of our Universe (e.g. Alpher et al., 1948; Dicke et al., 1965). Measuring the energies of a set of photons along any line-of-sight through the CMB will produce a Planck distribution with a characteristic energy[2] of 2.7 K, with a maximum deviation of $\pm$ 200 $\mu$K along any other line-of-sight. The fact that the fluctuations are so small leads to the assumption that the universe must have been much smaller early after its formation and then rapidly inflated (e.g. Guth, 1981). The fact that there are fluctuations at all suggest that our universe was not completely homogenized, but had primordial fluctuations in the matter-radiation plasma of the early universe that were 'frozen' out during this expansion. These density perturbations seeded the first objects that would eventually collapse under gravity to form the structure of our universe.

The first component to de-couple from the primordial plasma was dark matter. For it to do so requires dark matter particles to be described by a non-relativistic fluid even at the extremely high temperatures in the early universe, suggesting relatively heavy particles (a few times the mass of the proton, e.g. Geringer-Sameth &

[2] In the Planck function, the characteristic energy is related to temperature through Boltzmann's constant.

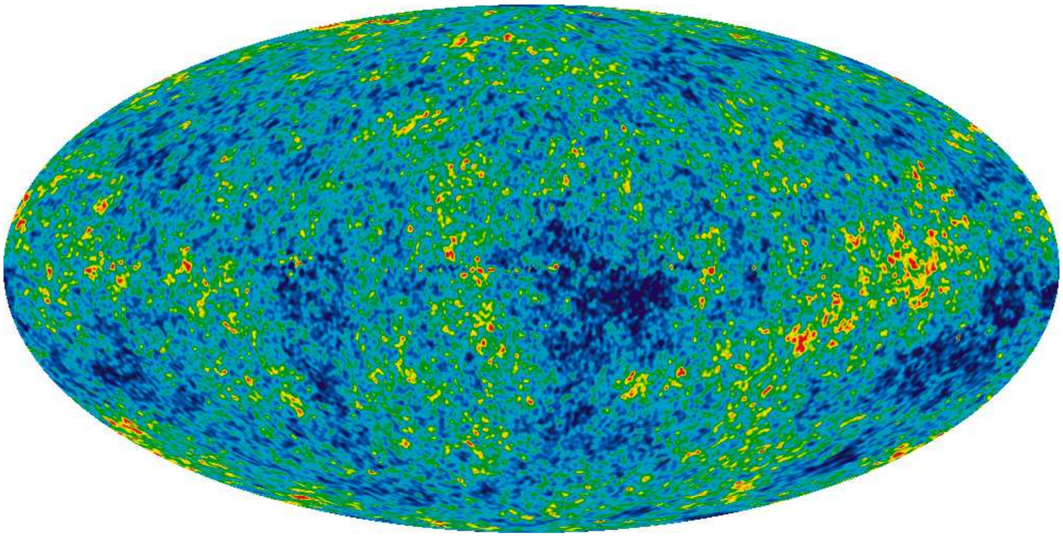

Figure 1.1: The Cosmic Microwave Background, as seen from the Wilkinson Microwave Anisotropy Probe (Bennett et al., 2013). The colour range, from blue to red, corresponds to a temperature deviation of -200 to +200 $\mu$K from the mean. *Image credit: Adapted from Figure 27 of Bennett, C. L. et al., 2013, "Nine-Year* Wilkinson Microwave Anisotropy Probe (WMAP) *Observations: Final Maps and Results", The Astrophysical Journal Supplement Series, Volume 208, Number 2, 54 pp. ©AAS. Reproduced with permission.*

Koushiappas, 2011). The luminous baryons, however, must cool adiabatically with the expansion of the universe before de-coupling from the thermal background of the universe (e.g. White & Rees, 1978). The now atomic gas — primarily hydrogen and helium — will experience dissipational collapse towards the centres of dark matter 'halos'.

The formation and evolution of a galaxy is a complicated process (see McKee & Ostriker, 2007, for a recent review). Gas must collapse and cool into very small structures, with densities above $\sim 100$ atoms cm$^{-3}$ and temperatures below 100 K (e.g. Di Francesco et al., 2007), in order to form stars. These structures are termed molecular clouds due to the fact that the majority of the mass is in molecular form and dominated by $H_2$. Surrounding these clouds is a multi-component Interstellar Medium (ISM) ranging from warm neutral gas to hot ionized plasma (e.g. McKee & Ostriker, 1977). At all these scales, from the small proto-disks surrounding young stars within which planets will form, to the large spiral structures of late-type galaxies, there is the interplay between gravity pulling everything down and magnetic fields, hydrodynamic forces, and angular momentum holding it all up.

On the other hand, dark matter is relatively free of the above effects. This is due to the fact that of the four fundamental forces of nature, dark matter particles couple strongly only to gravity[3]. As a collisionless fluid, the seeds of dark matter halos form from dissipationless gravitational collapse. Once a halo virialises, it can only collapse to higher densities through two body scattering. Growth of a dark matter halo comes through a hierarchical process, where the smallest halos are the first to collapse out of the Hubble flow, before merging into successively larger halos with time (see Frenk & White, 2012, for a recent review). This is illustrated in Figure 1.2.

## 1.2 The Structure of Dark Matter Halos

The process of dark matter halo formation requires following the collisionless fluid of particles in the six-dimensional phase space (a function of $\vec{r}$ and $\vec{v}$) through time. In the early universe, the density fluctuations in the dark matter can be modelled as small spherical perturbations within the background mean:

$$\rho(t) = \bar{\rho}(t)[1 + \delta(t)]. \tag{1.1}$$

[3]In a stricter sense, dark matter particles also couple via the electroweak force as they are predicted to undergo particle-antiparticle annihilation but at a level much lower than that of the cosmic background (e.g. Gunn et al., 1978; Geringer-Sameth & Koushiappas, 2011). There are a number of experiments whose goal is the direct detection of the dark matter particle (e.g. Bergström, 2013).

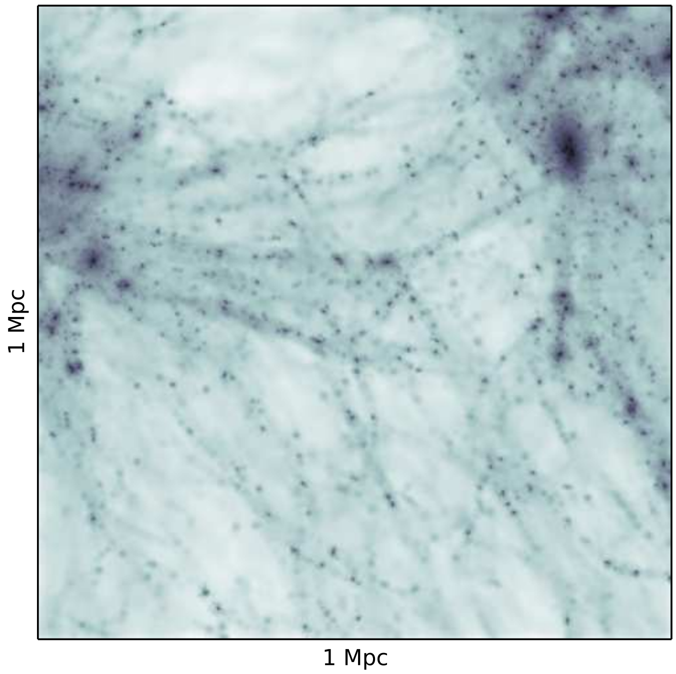


Figure 1.2: The growth of dark matter structures in the Universe. This particular simulation was run until the universe was about 3 Gyr old. The darker regions correspond to the highest projected densities. Notice the filaments of structure, within which tiny halos have collapsed. Smaller halos will end up being fed to the larger halos at filament intersections.

Following the collapse of an over dense region in the early universe means solving for the time evolution of $\delta(t)$ under the following initial condition:

$$0 < \delta(t_o) << 1. \tag{1.2}$$

In this 'linear' regime it is straightforward to write down analytic approximations for the growth of $\delta(t)$. Once the collapse approaches the non-linear regime ($\delta(t) \gtrsim 1$), numerical integration is required (e.g. Peebles, 1987). For example, the direct evolution of the six-dimensional phase space (e.g. Widrow, 1997; Dehnen, 2005, see also Widrow & Kaiser 1993 who use an alternative method) through time will provide information on the density structure of halos. However, numerical simulations provide a powerful and straightforward tool for studying dark matter halos.

### 1.2.1 Simulations

In principle, numerical simulations of the formation of dark matter halos are straightforward. The initial conditions are set by measuring the relative strength of the density fluctuations present in the CMB (by taking the Fourier transform e.g. Hinshaw et al., 2013) and evolving dark matter particles[4] under gravity. Many of these simulations (e.g. Bullock et al., 2001; Klypin et al., 2001; Stadel et al., 2009) suggest one singular profile for the dark matter density distribution, regardless of halo mass:

$$\rho(r) = \frac{\rho_{\rm c}\delta_c}{\frac{r}{r_{\rm s}}(1+\frac{r}{r_{\rm s}})^2}. \tag{1.3}$$

This density profile is colloquially known as the NFW profile after the authors that first showed its applicability to dark matter halos in a series of influential papers (Navarro et al., 1995, 1996b, 1997). The first parameter, $\rho_{\rm c}$, is the critical density of the universe, defined as the total mass density required for the universe to be flat. The two best fit parameters are $\delta_c$, a normalization constant, and $r_s$, a scale radius. Although other density profiles have been proposed (such as the Einasto 1965 profile e.g. Ludlow et al., 2013) the main feature of the dark matter halo is the presence of an inner cusp (e.g. the Navarro et al., 1997, result that $\rho \propto r^{-1}$).

There is a significant limitation to the NFW density profile, though, in that

[4]Computational limits force simulations to use a single particle to represent $\sim 10^3\,{\rm M}_\odot$ of individual dark matter particles.

it does not yield a finite mass:

$$M(r) = \int_0^r 4\pi r'^2 \rho(r')\mathrm{d}r' = 4\pi\rho_\mathrm{c}\delta_\mathrm{c} r_\mathrm{s}^3[\ln(\frac{r}{r_\mathrm{s}}+1) - \frac{r}{r+r_\mathrm{s}}]. \tag{1.4}$$

One would expect that this density distribution would break at the outer edge of the halo and transition to the cosmic dark matter background (i.e. the web in Figure 1.2). An oft-used estimate of this edge can be made by making the assumption that the density fluctuations present in the early universe can be treated as spherical regions of uniform density (the so-called 'spherical top-hat') and following its collapse under gravity. The halo radius, $r_\mathrm{h}$, is then defined as the region within which a halo of mass $M_\mathrm{h}$ has virialised after collapse. If the mean density of the halo is defined as:

$$\bar{\rho}_\mathrm{h} \equiv \frac{M_\mathrm{h}}{\frac{4\pi}{3} r_\mathrm{h}^3}, \tag{1.5}$$

then the solution to the top-hat collapse suggests that:

$$\Delta_\mathrm{c} = \frac{\bar{\rho}_\mathrm{h}}{\rho_\mathrm{c}}. \tag{1.6}$$

This constraint defines the halo mass and radius. Since $\Delta_\mathrm{c}$ represents the density of the halo that collapses out of the Hubble flow, it depends sensitively on the matter density of the universe as it expands, and thus on the particular cosmology one assumes[5].

The other free parameter, $r_\mathrm{s}$, represents the mid-point of the transition from the $r^{-3}$ density profile in the outer regions to the $r^{-1}$ in the inner regions. Since dark matter halos undergo collisionless mergers, $r_\mathrm{s}$ depends on the merger history of the

[5]For $z \gtrsim 4$ it takes the value of $18\pi^2$, which is why in the literature $r_\mathrm{h}$ and $M_\mathrm{h}$ are replaced with $r_{200}$ and $M_{200}$, respectively. See Bryan & Norman (1998) for an example of a functional fit to $\Delta_\mathrm{c}$ as a function of $z$.

present day halo; some halos may be more centrally concentrated than other halos. If we defined the concentration parameter $c$ as the ratio $r_{\rm h}/r_{\rm s}$, then irrespective of halo mass we can combine Equations (1.4), (1.5), and (1.6) to find:

$$\delta_{\rm c} = \Delta_{\rm c} \frac{c^3}{3[\ln{(c+1)} - \frac{c}{c+1}]} \tag{1.7}$$

Thus, for a given cosmology and using the assumption of top-hat collapse, one can describe a particular NFW halo with a two parameter fit in $M_{\rm h}$-$c$.

### 1.2.2 Observations

The evidence for dark matter has come primarily from its gravitational effects on luminous (baryon) matter. The first hint that a significant fraction of the matter in the universe is dark was found by Zwicky (1933), who showed that the gravitational mass of a galaxy cluster was much larger than the luminous mass inferred from the observed starlight. Four decades later, observations of the rotation of late-type spirals showed that galaxies must be significantly dominated by a dark matter component. In a Keplerian system — that is, a system in which the scalar gravitational potential is given by $1/r$ — the rotation speed $v$ of a particle about the total mass $M(r)$ within $r$ is given by:

$$v(r) = \sqrt{\frac{GM(r)}{r}} \tag{1.8}$$

The pivotal work of Rubin et al. (1978, 1980) and Bosma (1981) showed that the galaxy rotation profiles were relatively flat out to the furthest observable point. If the majority of the mass of a galaxy were contained in stars, then the expected mass profile would be similar to the exponentially decreasing surface brightness profile (e.g. de Vaucouleurs, 1948; Sérsic, 1963). Instead, the outer rotation rate of these galaxies suggested density profiles of $\rho \propto r^{-3}$, which would subsequently be predicted by numerical experiments.

Unfortunately, dynamical systems of stars moving in a gravitational potential generally show more complicated motion than that of a uniformly rotating disk. In these cases, measuring the kinematic properties of collisionless particles — stars — can constrain the galactic potential so long as the six-dimensional phase space density is conserved (e.g. Jeans, 1915; Binney & Tremaine, 2008). These properties — density, position, and velocity — can be measured from photometry and spectroscopy. However, the galactic potential determined using the series of differential equations outlined in Jeans (1915) describes the total mass density distribution, that is, the sum of both luminous and dark matter components; only in dark matter dominated systems will the galactic potential be almost completely defined by the dark matter density distribution.

One straightforward observational estimate of the baryon contribution to the galactic potential is to divide the total gravitational mass of the galaxy by its power output — the mass-to-light ratio — since dark matter dominated systems will have the largest values. Galaxies like our own Milky Way have high mass-to-light ratios and high stellar densities near their centres, making it difficult to probe the inner regions of the host dark matter halos. Dwarf galaxies — the low mass end of the galaxy spectrum — present a much more palatable target. Since these galaxies host so few stars, and show very little star formation in the last few Gyr (e.g. Mateo, 1998; McConnachie, 2012), they truly represent dark matter dominated systems (e.g. Dekel & Silk, 1986) and are the fossils of massive galaxy formation (e.g. White & Rees, 1978). Plenty of dwarf galaxies make up the Local Group of galaxies surrounding the Milky Way; an example of a Local Group Dwarf Spheroidal

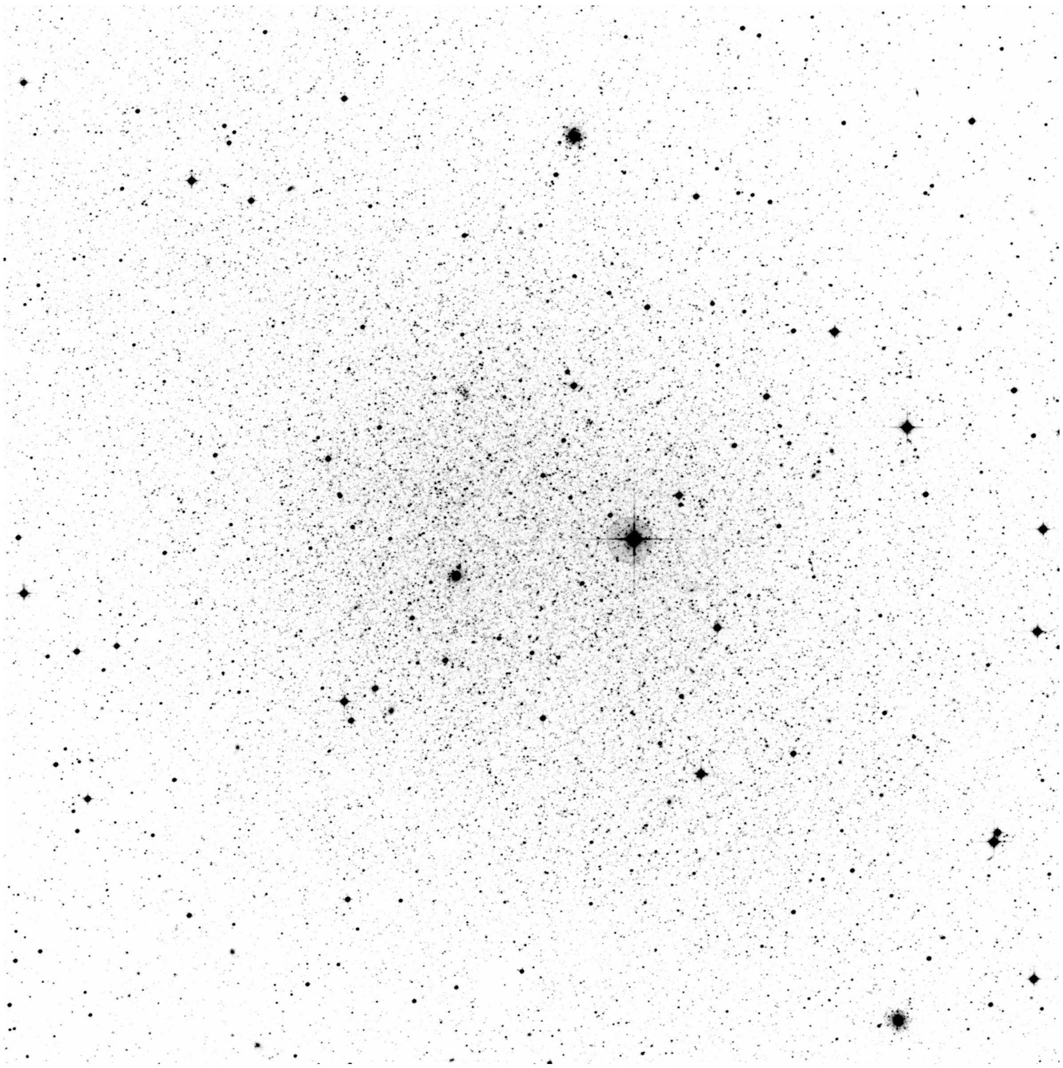

Figure 1.3: An R-band $45\times45$ arcminute ($1820\times1820$ pc or $6000\times6000$ ly) image of Fornax, a Dwarf Spheroidal in the Local Group of galaxies. Many dwarf galaxies only host $10^4$–$10^7$ stars over a wide area, and so show up as a small over-density of stars against the foreground Milky Way stars (e.g. Ibata et al., 1995). Fornax hosts five Globular Clusters, three of which can be seen in the image (bottom right, top centre, and to the East of the brightest star). *Image credit: POSS-II / CalTech / AAO / ROE / STScI*

galaxy, Fornax, is shown in Figure 1.3.

The first papers inferring the density profiles for a number of dwarf galaxies (e.g. Flores & Primack, 1994; Moore, 1994) began to challenge the assumption that all dark matter halos must follow the NFW profile. Instead of the cuspy density profiles predicted in cold dark matter simulations, the data argued for constant (i.e. cored) density profiles within the inner 100–1000 pc, shown in Figure 1.4. Many dwarf galaxies both within our local group and without exhibit this constant density behaviour, suggesting that there is some internal mechanism (as opposed to the environment in which the galaxy lives) that either destroys cusps or prevents them from forming (e.g. Gilmore et al., 2007). This cusp-core discrepancy posed a serious challenge to the simple cosmological model discussed above (see de Blok, 2010, for a recent review).

#### 1.2.2.1 Further Problems with ΛCDM

The cusp-core problem is not the only challenge for the ΛCDM paradigm. Both semi-analytic (e.g. Kauffmann et al., 1993) and numerical (e.g. Klypin et al., 1999; Moore et al., 1999) models of galaxy formation over-predict the number of satellite galaxies around Milky Way and Local Group analogues — the *missing satellites* problem. More recently, Boylan-Kolchin et al. (2011) found that the most massive and dense dark matter sub-halos predicted in dissipationless simulations could not host the brightest Milky Way satellites — yet they are *too big to fail* to form stars. Although this thesis focuses solely on answering the cusp-core problem, many of these challenges require solutions similar to that discussed below.

## 1.3 Resolving The Discrepancy

We require a solution to the cusp-core discrepancy within the current cosmological paradigm. Either modifications must be made to the dark matter model, or previously ignored baryon processes are modifying the dark matter structures.

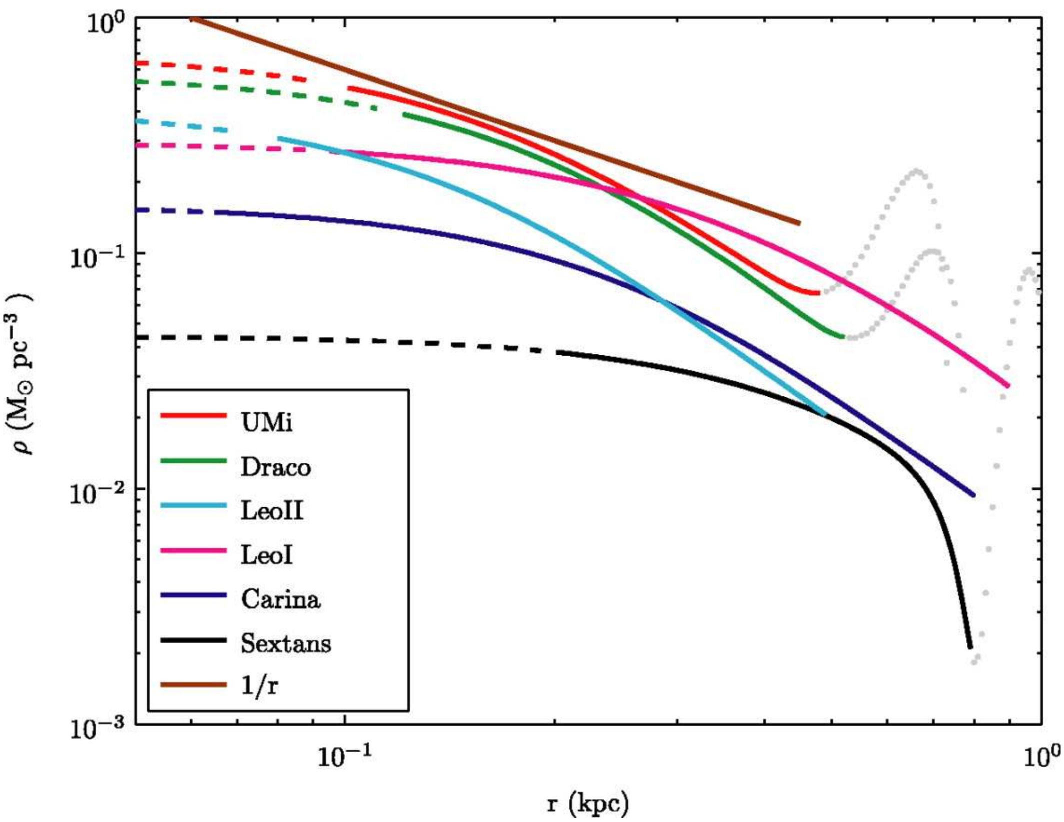


Figure 1.4: The inferred mass density distribution of a set of dwarf galaxies within our local group. These dwarf galaxies are inconsistent with the cusped $r^{-1}$ density profile shown. *Image credit: Adapted from Figure 4 of Gilmore, G. et al., 2007, "The Observed Properties of Dark Matter on Small Spatial Scales", The Astrophysical Journal, Volume 663, Number 2, pp. 948–959. ©AAS. Reproduced with permission.*

### 1.3.1 Heating up Cold Dark Matter

A complete theory of the dark matter particle must be able to satisfy observational constraints on all scales. For over thirty years, observational undertakings such as the Harvard-Smithsonian Centre for Astrophysics redshift survey (Davis et al., 1982; Huchra et al., 1983) and the Sloan Digital Sky Survey (York et al., 2000; Abazajian et al., 2003) have mapped out the distribution of luminous galaxies as a function of $z$, the cosmological redshift. Since the universe has been expanding from the Hot Big Bang, the measured cosmological redshift of a given galaxy translates directly to a physical distance[6]. Assuming a one-to-one mapping between galaxies and dark matter halos, the large scale structure of dark matter suggests that it is highly clustered, with long filaments and large bubbles devoid of structure.

The thermal properties of dark matter particles as they decoupled from the rest of the primordial plasma directly affect the structural properties of dark matter halos on all scales. As the average dark matter particle velocity increases[7] small scale structure is wiped out, since dark matter particles can now escape from the low mass over-density perturbations as they collapse out of the Hubble flow. This hot dark matter universe undergoes top-down structure formation since the first structures to form are large scale filaments or pancakes, inside of which dark matter halos fragment out relatively late; structure formation is suppressed for $z \gtrsim 5$. On the other hand, a cold dark matter universe undergoes bottom-up formation as the first structures that form are the small halos, which then merge into larger halos as they collapse from the voids into filaments, and then as the filaments flow into nodes. In the CDM picture, rich galaxy clusters are found in these nodes, where many filaments interact, whereas isolated galaxies are found primarily in the voids. Simulations of the formation of large scale dark matter structure where the temperature of the dark matter particle is varied have confidently ruled out hot particles (e.g. Colombi et al., 1996).

Warm dark matter — essentially a midway point between the two extremes — is still plausible. By making dark matter warm, the smallest scale fluctuations in the dark matter density field are still suppressed; this simultaneously inhibits the growth of the smallest halos and smears out the central cusps but exhibits all the large scale properties of dark matter halos (e.g. Hogan & Dalcanton, 2000; Bode

[6]The relation between $z$ and distance depends on the chosen cosmological model.
[7]In other words, as the dark matter temperature increases.

et al., 2001; Frenk & White, 2012; Lovell et al., 2014). One could also introduce a new self-interaction between dark matter particles (e.g. Spergel & Steinhardt, 2000) that could smooth out the inner cusps (e.g. Vogelsberger et al., 2012). However, warm dark matter may not actually solve some of the observations that currently challenge cold dark matter (e.g. Schneider et al., 2014) or form the large cores observed in nature (e.g. Macciò et al., 2012). Furthermore, using warm dark matter to suppress small scale halos inhibits the formation of stars, in turn delaying the onset of reionization much later than currently expected (e.g. Somerville et al., 2003).

### 1.3.2 Adding Baryons

Since baryons can undergo dissipational collapse, the gas density can grow to extremely large values and significantly slow down computations. However, collisionless dark matter particles require many Hubble times to reach the same densities since they can only collapse through two-body scattering. A computer simulation with hundreds of millions of dark matter particles can evolve much faster and achieve acceptable resolution, utilizing a number of different numerical schemes to solve Newton's equations of motion under gravity.

For a parcel of gas, continual collapse under gravity will lead to the process of star formation. Although stars themselves are collisionless particles (like dark matter), there is significant energy associated with their formation. Most stars form in a cluster (e.g. Lada & Lada, 2003) with a wide range of initial masses (e.g. Salpeter, 1955; Miller & Scalo, 1979; Kroupa, 2001; Chabrier, 2003); luminosity, size, lifetime, and temperature are directly related to the initial mass of a star. The most massive stars are also the brightest and hottest, emitting significant amounts of ionizing flux and radiation pressure. These massive stars evolve very quickly (in roughly 5 Myr as opposed to the 10 Gyr lifetime of our own Sun) before exploding as supernovae. A single supernova releases about $10^{51}$ ergs of energy, which can then heat the surrounding interstellar medium above $10^6$ K and blow winds upwards of $100\,\mathrm{km\,s^{-1}}$.

Usually, 'sub-grid' recipes are used to model the star formation process as many hydrodynamic simulations of galaxies do not fully resolve all the necessary scales. A simple and effective model commonly used takes as input the gas density and mass in the region defined by the smallest resolution length. Although there are many processes that affect the rate at which stars form, the efficiency is related to density via a power law of the form (Schmidt, 1959, 1963, see Kennicutt & Evans 2012 for a recent review):

$$\dot{\rho}_{\mathrm{SF}} = C_* \rho_{\mathrm{g}}^n. \tag{1.9}$$

Here, $\dot{\rho}_{\mathrm{SF}}$ is the star formation rate density, and $\rho_{\mathrm{g}}$ is the local gas density. The index $n$ is typically taken to be 1.5 to reflect that the process of star formation happens upon the a timescale proportional to ${\rho_{\mathrm{g}}}^{-1/2}$, and $C_*$ is an efficiency parameter tuned to match observations. The rate at which stars form then sets the amount of feedback energy that is dumped back into the surrounding gas — for example, by heating the gas to a specific temperature — in the simulation. Many of the more sophisticated star formation and feedback recipes are built from this (e.g. Gnedin et al., 2009; Hopkins et al., 2011; Christensen et al., 2012; Agertz et al., 2013; Hopkins et al., 2013; Keller et al., 2014).

One of the first studies of how baryons affect the structure of dark matter halos was undertaken by Navarro et al. (1996a). A decade previously Dekel & Silk (1986) had argued that the formation of the diffuse stellar surface densities in dwarf galaxies was a result of the feedback from supernovae. Since the typical escape velocity of dwarf galaxies is on the order of the supernova wind speed, they experienced significant bouts of gas loss with each burst of star formation. Navarro et al. (1996a) considered an analytic approximation of a galactic disk potential implanted in a dark matter halo, and the gas blow-out was modelled by instantaneously removing the potential. Once the dark matter halo settled back towards equilibrium, the central density profile had transitioned from a cuspy $r^{-1}$ dependence to a relatively flat constant density core. Further work using slightly more realistic models of the gas outflow supported this conclusion (e.g. Read & Gilmore, 2005).

Given the impractical assumption of complete instantaneous blowout in the Navarro et al. (1996a) picture of core formation, other groups were motivated to find more realistic ways in which to transfer energy and angular momentum from the collapsing baryons to the dark matter particles within the cusp. Weinberg & Katz (2002) proposed that a gaseous/stellar bar [8], an unstable mode that can develop in thin disks of particles (e.g. Hohl, 1971; Binney & Tremaine, 2008), could essentially stir up the dark matter, by creating a gravitational wake as it rotated. However, a significant amount of baryon matter is required to grow a bar, and its transient nature combined with the deepening of the central potential as the baryons accumulated in the centre of the halo was shown to inhibit the formation of a core (e.g. Sellwood, 2003; Dubinski et al., 2009).

El-Zant et al. (2001) proposed that discrete massive clumps of gas accreting onto the dark matter halo could remove the cusp through a process called dynamical friction: as a massive particle moves through a sea of lower mass particles, there is a gravitational 'wake' formed behind the massive particle. This wake then slows down the massive particle; the result is energy is transferred from the massive parti-

[8] the requirement that galactic disks be stable to large bars supports the idea that a significant fraction of the mass in our galaxy is dark (e.g. Ostriker & Peebles, 1973).

cle to the sea of lower mass particles. However, this process is most efficient when the in-falling gas is resolved in a small number of large mass clumps (each $\gtrsim 0.5\%$ of the halo mass, e.g. Jardel & Sellwood, 2009).

An attractive modification to the Navarro et al. (1996a) model was suggested by Mashchenko et al. (2006). The thermal feedback on the surrounding dense gas by supernovae formed in dense stellar clusters will drive massive outflows from the centre of the halo. However, contrary to the complete thermal blow-out advocated by Navarro et al. (1996a) and Read & Gilmore (2005), bulk motion is driven in the gas both before and after the star formation burst, sloshing around the centre of the dark matter halo before being expelled from the inner cusp. This rapidly changes the gravitational potential within the centre of the halo, which in turn changes the orbital energy of the dark matter particles within the halo (Lynden-Bell, 1967; Pontzen & Governato, 2012). The novelty in this picture is that it is much more energetically feasible: multiple star formation events provide the perturbations to the potential, and thus the dark matter orbits, without having to completely drive gas out of the halo. A subsequent cosmological simulation studied in Mashchenko et al. (2008) verified that the process formed a realistic cored dwarf galaxy using standard prescriptions for sub-grid star formation. A simple toy model is discussed below.

#### 1.3.2.1 A Toy Model

A simple toy model can be built by setting up $N$ massless particles in orbit around a particle of mass $m_o$. This is an acceptable model of a dark matter halo, since the total halo mass is much greater than the individual dark matter particle mass. In the Mashchenko et al. (2006) picture, the gravitational potential fluctuates rapidly through the combined processes of hierarchichal accretion, star formation, and gas bulk motions. Here, this is approximated by setting $m_o \to m(t)$, that is, the central mass now becomes some function of $t$. In principle, this function $m(t)$ is extremely complicated, however as discussed in Chapter 3 the behaviour is approximately cyclic; thus, a simple approximation to a burst of star formation is a sinusoidal function:

$$m(t) = m_o[1 - f \sin^2(\omega t)], \tag{1.10}$$

where $f$ and $\omega$ are the amplitude and frequency of the oscillation in mass.

Figure 1.5 shows the evolution of the orbit and energy for one of these massless particles as a function of time in units of the initial period of the orbit. The bottom panel of the figure shows how the central mass evolves under Equation (1.10): the black line shows an adiabatically varying mass, the gray dashed line shows two top-hat 'blow-outs' (as in Pontzen & Governato, 2012), while the solid gray line shows a sinusoidal variation. In the adiabatic and sinusoidal cases, the amplitude $f$ was chosen to be a 5% reduction in the central mass, while the top-hat was set to half of this value (the time average over one period of oscillation). The variations in $m(t)$ begin and end at set times, and $\omega$ was chosen to give an integer number of oscillations. The top and middle panels show the evolution of the orbit and orbital energy, respectively; a positive increase in $E(t)$ corresponds to a particle gaining energy. Adiabatic changes to the gravitational potential — those that occur on timescales much longer than the orbital period — lead to reversible changes in the orbital energy; the particle ends up on the same orbit as before the change. Irreversible changes occur when the potential fluctuations occur on short timescales, and the net energy gain (or loss) of the particle is clearly dependent on the timescale of these changes. Rapid fluctuations are indistinguishable from an impulsive blowout (as expected from the time average of a sinusoidal) but fluctuations commensurate with particle orbital times can drive significant energy gains.

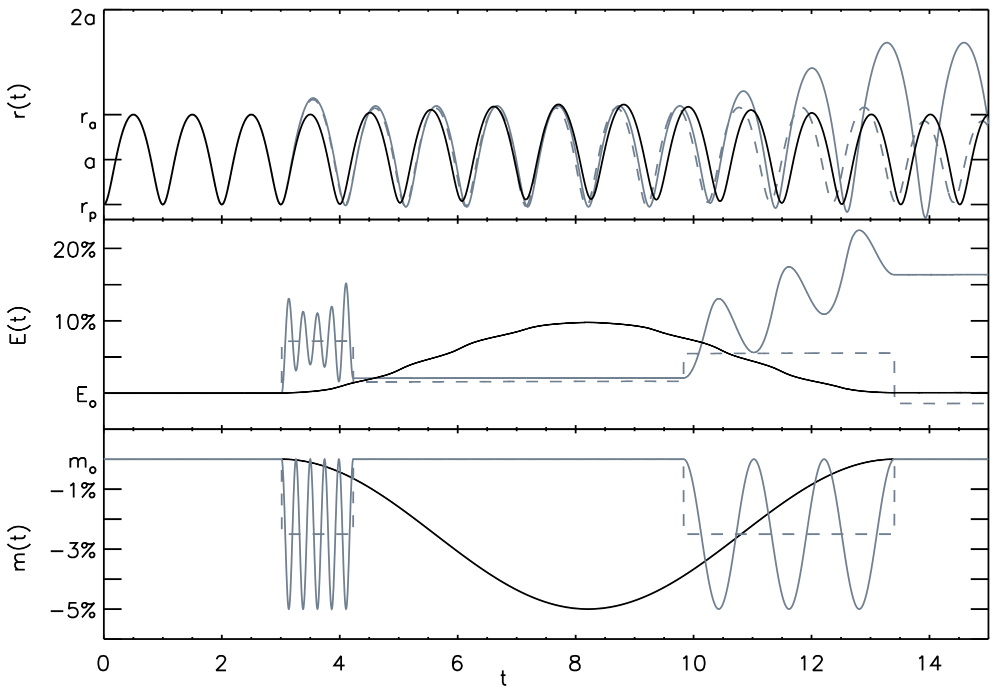


Figure 1.5: The evolution of the Keplerian orbit whose central mass varies with time as shown by Equation (1.10). *Top*: The orbital radius as a function of time. The initial semi-major axis $a$ as well as the closest and furthest points from the central mass, $r_p$ and $r_a$, are marked. *Middle*: The orbital energy. Each vertical tick represents a loss or gain of 5% of the initial orbital energy, $E_o$. *Bottom*: The variation of the central mass as a function of time.

Since the change in energy of the particle also depends on the phase of its orbit, averaging over many fluctuations at various phases of the orbit will result in a net energy gain.

### 1.3.3 Objections to Star Formation Feedback

Much work has been done to determine how efficiently bulk motions driven in dense star forming gas from stellar feedback can grow dark matter particle orbits. Many cosmological simulations of dwarf galaxies have invoked star formation feedback, usually only from supernovae, to explain the formation of dark matter cores in the halos (e.g. Governato et al., 2010, 2012; Teyssier et al., 2013; Governato et al., 2014; Shen et al., 2013; Madau et al., 2014; Di Cintio et al., 2014). This process also provides an attractive solution to both the *Missing Satellites* (e.g. Brooks et al., 2013) and the *Too Big To Fail* (e.g. Zolotov et al., 2012; Brooks & Zolotov, 2014) problems; lowering the central densities of dark matter halos reduces their rotation velocities, increases the susceptibility of dwarfs to disruption by gravitational tides, and induces star formation quenching via gas expulsion and stripping. Observational predictions of the core formation process have also been made for the stellar distribution (Teyssier et al., 2013) and the relation between total stellar mass and halo mass (Di Cintio et al., 2014). An analytic description of the process has been given by Pontzen & Governato (2012).

Despite these successes, many authors have demonstrated caveats to the process of dark matter core formation outlined in Mashchenko et al. (2006) and Mashchenko et al. (2008) that must be understood. Factors such as how much mass is ejected per star formation event (e.g. Garrison-Kimmel et al., 2013) and the time scale on which the mass is removed from the centre (e.g. Ogiya & Mori, 2011) significantly affect the ability of a given halo to become cored. Boylan-Kolchin et al. (2012) argued that simulations tend to produce over-luminous dwarf galaxies when trying to match the central dark matter densities. For star formation feedback to be an acceptable source of energy to be pumped into the dark matter, simulations need to be able to match all the properties of LGDs including both the core radius and the stellar masses. These arguments show that it is unclear how efficient the stellar feedback energy can couple to the dark matter particles via the induced potential fluctuations.

In the broadest sense the coupling efficiency is the fraction $\epsilon$ of the supernova energy that is converted to the orbital energy of dark matter particles.

Rather than study a cosmological simulation or a controlled numerical experiment, Peñarrubia et al. (2012) used analytic arguments based on simple approximations of the system to calculate $\epsilon$ for a given dark matter halo mass and core size. Assuming:

- a relation between the galaxy stellar mass and dark matter halo mass, and
- the amount of energy required to convert a cusp into a core was the difference between the gravitational potential energies of each halo,

Peñarrubia et al. argued that even with an efficiency as high as 40 per cent it would be impossible for supernovae alone to create cores in dwarf galaxies, and thus star formation feedback could not solve the $\Lambda$CDM cusp-core problem.

## 1.4 This Thesis

Clearly, there is still significant work to be done on the cusp-core problem in dark matter halos. However, the observational consequences of the Mashchenko et al. (2006) core formation paradigm have not been studied in much detail; this thesis aims to study how the stellar component of dwarf galaxies would be affected if this process was indeed taking place. Since both stars and dark matter are collisionless particles, they should both evolve in the same manner — stars that form in the centre of a dark matter halo will also have their orbits grown. This process is instrumental in shaping the current stellar distribution of dwarf galaxies, and as such of the massive galaxies built via accretion. It will also affect the enrichment history of gas within dwarf galaxies and the surrounding intergalactic medium. The novelty in this approach is that it strengthens the argument that cores evolve from cusps through baryon influence by tying previously unrelated problems together into a coherent picture of dwarf galaxy evolution and star formation.

The organization of this thesis is as follows. I first show that the supernova energy available from the average stellar population in a dwarf galaxy is enough to create a sizable dark matter core, and use these calculations to begin to constrain how efficient the core formation process is in Chapter 2. Although this was the final paper submitted for publication during my thesis, it motivates the first two papers. In Chapter 3 I show that the energy from stellar feedback is transferred both to the dark matter and the stellar population within the centre of the dark matter halo, which reproduces a broad range of observational features of the local group dwarf galaxies. In Chapter 4, I focus directly on the evolution of the globular cluster population forming in dwarf galaxies and show that their history of element enrichment via evolving stars is consistent with this picture of dark matter core formation. I provide a summary of these results and discuss future work in Chapter 5.

# Bibliography

Abazajian, K., Adelman-McCarthy, J. K., Agüeros, M. A., et al. 2003, AJ, 126, 2081

Agertz, O., Kravtsov, A. V., Leitner, S. N., & Gnedin, N. Y. 2013, ApJ, 770, 25

Alpher, R. A., Bethe, H., & Gamow, G. 1948, PhRv, 73, 803

Bennett, C. L., Larson, D., Weiland, J. L., et al. 2013, ApJS, 208, 20

Bergström, L. 2013, Physica Scripta Volume T, 158, 014014

Binney, J., & Tremaine, S. 2008, Galactic Dynamics: Second Edition (Princeton University Press)

Bode, P., Ostriker, J. P., & Turok, N. 2001, ApJ, 556, 93

Bosma, A. 1981, AJ, 86, 1825

Boylan-Kolchin, M., Bullock, J. S., & Kaplinghat, M. 2011, MNRAS, 415, L40

—. 2012, MNRAS, 422, 1203

Brooks, A. M., Kuhlen, M., Zolotov, A., & Hooper, D. 2013, ApJ, 765, 22

Brooks, A. M., & Zolotov, A. 2014, ApJ, 786, 87

Bryan, G. L., & Norman, M. L. 1998, ApJ, 495, 80

Bullock, J. S., Kolatt, T. S., Sigad, Y., et al. 2001, MNRAS, 321, 559

Chabrier, G. 2003, PASP, 115, 763

Christensen, C., Quinn, T., Governato, F., et al. 2012, MNRAS, 425, 3058

Colombi, S., Dodelson, S., & Widrow, L. M. 1996, ApJ, 458, 1

Davis, M., Huchra, J., Latham, D. W., & Tonry, J. 1982, ApJ, 253, 423

de Blok, W. J. G. 2010, AdAst, 2010

de Vaucouleurs, G. 1948, Annales d'Astrophysique, 11, 247

Dehnen, W. 2005, MNRAS, 360, 892

Dekel, A., & Silk, J. 1986, ApJ, 303, 39

Di Cintio, A., Brook, C. B., Macciò, A. V., et al. 2014, MNRAS, 437, 415

Di Francesco, J., Evans, II, N. J., Caselli, P., et al. 2007, Protostars and Planets V, 17

Dicke, R. H., Peebles, P. J. E., Roll, P. G., & Wilkinson, D. T. 1965, ApJ, 142, 414

Dubinski, J., Berentzen, I., & Shlosman, I. 2009, ApJ, 697, 293

Einasto, J. 1965, TrAlm, 5, 87

El-Zant, A., Shlosman, I., & Hoffman, Y. 2001, ApJ, 560, 636

Flores, R. A., & Primack, J. R. 1994, ApJL, 427, L1

Frenk, C. S., & White, S. D. M. 2012, Annalen der Physik, 524, 507

Garrison-Kimmel, S., Rocha, M., Boylan-Kolchin, M., Bullock, J. S., & Lally, J. 2013, MNRAS, 433, 3539

Geringer-Sameth, A., & Koushiappas, S. M. 2011, Phys. Rev. Lett., 107, 241303

Gilmore, G., Wilkinson, M. I., Wyse, R. F. G., et al. 2007, ApJ, 663, 948

Gnedin, N. Y., Tassis, K., & Kravtsov, A. V. 2009, ApJ, 697, 55

Governato, F., Brook, C., Mayer, L., et al. 2010, Nature, 463, 203

Governato, F., Zolotov, A., Pontzen, A., et al. 2012, MNRAS, 422, 1231

Governato, F., Weisz, D., Pontzen, A., et al. 2014, arXiv:1407.0022

Gunn, J. E., Lee, B. W., Lerche, I., Schramm, D. N., & Steigman, G. 1978, ApJ, 223, 1015

Guth, A. H. 1981, PhRvD, 23, 347

Hinshaw, G., Larson, D., Komatsu, E., et al. 2013, ApJS, 208, 19

Hogan, C. J., & Dalcanton, J. J. 2000, PhRvD, 62, 063511

Hohl, F. 1971, ApJ, 168, 343

Hopkins, P. F., Keres, D., Onorbe, J., et al. 2013, arXiv:1311.2073

Hopkins, P. F., Quataert, E., & Murray, N. 2011, MNRAS, 417, 950

Huchra, J., Davis, M., Latham, D., & Tonry, J. 1983, ApJS, 52, 89

Ibata, R. A., Gilmore, G., & Irwin, M. J. 1995, MNRAS, 277, 781

Jardel, J. R., & Sellwood, J. A. 2009, ApJ, 691, 1300

Jeans, J. H. 1915, MNRAS, 76, 70

Kauffmann, G., White, S. D. M., & Guiderdoni, B. 1993, MNRAS, 264, 201

Keller, B. W., Wadsley, J., Benincasa, S. M., & Couchman, H. M. P. 2014, MNRAS, 442, 3013

Kennicutt, R. C., & Evans, N. J. 2012, ARA&A, 50, 531

Klypin, A., Kravtsov, A. V., Bullock, J. S., & Primack, J. R. 2001, ApJ, 554, 903

Klypin, A., Kravtsov, A. V., Valenzuela, O., & Prada, F. 1999, ApJ, 522, 82

Kroupa, P. 2001, MNRAS, 322, 231

Lada, C. J., & Lada, E. A. 2003, ARA&A, 41, 57

Lovell, M. R., Frenk, C. S., Eke, V. R., et al. 2014, MNRAS, 439, 300

Ludlow, A. D., Navarro, J. F., Boylan-Kolchin, M., et al. 2013, MNRAS, 432, 1103

Lynden-Bell, D. 1967, MNRAS, 136, 101

Macciò, A. V., Paduroiu, S., Anderhalden, D., Schneider, A., & Moore, B. 2012, MNRAS, 424, 1105

Madau, P., Shen, S., & Governato, F. 2014, ApJL, 789, L17

Mashchenko, S., Couchman, H. M. P., & Wadsley, J. 2006, Nature, 442, 539

Mashchenko, S., Wadsley, J., & Couchman, H. M. P. 2008, Science, 319, 174

Mateo, M. L. 1998, ARA&A, 36, 435

McConnachie, A. W. 2012, AJ, 144, 4

McKee, C. F., & Ostriker, E. C. 2007, ARA&A, 45, 565

McKee, C. F., & Ostriker, J. P. 1977, ApJ, 218, 148

Miller, G. E., & Scalo, J. M. 1979, ApJS, 41, 513

Moore, B. 1994, Nature, 370, 629

Moore, B., Ghigna, S., Governato, F., et al. 1999, ApJL, 524, L19

Navarro, J. F., Eke, V. R., & Frenk, C. S. 1996a, MNRAS, 283, L72

Navarro, J. F., Frenk, C. S., & White, S. D. M. 1995, MNRAS, 275, 720

—. 1996b, ApJ, 462, 563

—. 1997, ApJ, 490, 493

Ogiya, G., & Mori, M. 2011, ApJL, 736, L2

Ostriker, J. P., & Peebles, P. J. E. 1973, ApJ, 186, 467

Peñarrubia, J., Pontzen, A., Walker, M. G., & Koposov, S. E. 2012, ApJL, 759, L42

Peebles, P. J. E. 1987, ApJ, 317, 576

Penzias, A. A., & Wilson, R. W. 1965, ApJ, 142, 419

Perlmutter, S., Aldering, G., Goldhaber, G., et al. 1999, ApJ, 517, 565

Planck Collaboration, Ade, P. A. R., Aghanim, N., et al. 2014, A&A, 571, A16

Pontzen, A., & Governato, F. 2012, MNRAS, 421, 3464

Read, J. I., & Gilmore, G. 2005, MNRAS, 356, 107

Riess, A. G., Filippenko, A. V., Challis, P., et al. 1998, AJ, 116, 1009

Rubin, V. C., Ford, W. K. J., & . Thonnard, N. 1980, ApJ, 238, 471

Rubin, V. C., Thonnard, N., & Ford, Jr., W. K. 1978, ApJL, 225, L107

Salpeter, E. E. 1955, ApJ, 121, 161

Schmidt, M. 1959, ApJ, 129, 243

—. 1963, ApJ, 137, 758

Schneider, A., Anderhalden, D., Macciò, A. V., & Diemand, J. 2014, MNRAS, 441, L6

Sellwood, J. A. 2003, ApJ, 587, 638

Sérsic, J. L. 1963, Boletin de la Asociacion Argentina de Astronomia La Plata Argentina, 6, 41

Shen, S., Madau, P., Conroy, C., Governato, F., & Mayer, L. 2013, arXiv:1308.4131

Somerville, R. S., Bullock, J. S., & Livio, M. 2003, ApJ, 593, 616

Spergel, D. N., & Steinhardt, P. J. 2000, PhRvL, 84, 3760

Stadel, J., Potter, D., Moore, B., et al. 2009, MNRAS, 398, L21

Teyssier, R., Pontzen, A., Dubois, Y., & Read, J. I. 2013, MNRAS, 429, 3068

Vogelsberger, M., Zavala, J., & Loeb, A. 2012, MNRAS, 423, 3740

Weinberg, M. D., & Katz, N. 2002, ApJ, 580, 627

White, S. D. M., & Rees, M. J. 1978, MNRAS, 183, 341

Widrow, L. M. 1997, PhRvD, 55, 5997

Widrow, L. M., & Kaiser, N. 1993, ApJL, 416, L71

York, D. G., Adelman, J., Anderson, Jr., J. E., et al. 2000, AJ, 120, 1579

Zolotov, A., Brooks, A. M., Willman, B., et al. 2012, ApJ, 761, 71

Zwicky, F. 1933, Helvetica Physica Acta, 6, 110

# Chapter 2

# The Energetics of Cusp Destruction

Aaron J. Maxwell, James Wadsley, and H. M. P. Couchman *Submitted to* The Astrophysical Journal*, manuscript no. ApJ96454*

## 2.1 Introduction

Collisionless simulations of dark matter halos in a $\Lambda$CDM cosmology consistently predict a density profile that diverges towards the centre (e.g. Dubinski & Carlberg, 1991; Navarro et al., 1995, 1997; Bullock et al., 2001; Klypin et al., 2001; Stadel et al., 2009) over a wide mass range. This profile typically rolls over to $\rho \propto r^{-3}$ at large radii where it is broadly consistent with the rotation curves of many late-type galaxies (e.g. Rubin et al., 1980; Bosma, 1981). However, the inner cusp (e.g. $\rho \propto r^{-1}$, Navarro et al., 1995) is *inconsistent* with observations of rotation profiles in dwarf galaxies both within the local group and beyond (e.g. Flores & Primack, 1994; Moore, 1994; Burkert, 1995; Côté et al., 2000; Kuzio de Naray et al., 2006; Gilmore et al., 2007; Kuzio de Naray et al., 2008; Oh et al., 2011; Walker & Peñarrubia, 2011; Amorisco et al., 2013; Adams et al., 2014), which are better fit with a constant density within the central kpc or so. Two classes of solutions have been proposed to resolve this discrepancy. The first suggests that coupling to baryons can reshape the dark matter cusp into a core (e.g. Navarro et al., 1996a; El-Zant et al., 2001; Weinberg & Katz, 2002; Read & Gilmore, 2005; Mashchenko et al., 2006). These solutions have met with some criticism (e.g. Sellwood, 2003; Tasitsiomi, 2003; Jardel & Sellwood, 2009; Dubinski et al., 2009; Peñarrubia et al., 2012), and so alternative models to $\Lambda$CDM have been suggested, such as 'warm' dark matter (e.g. Hogan & Dalcanton, 2000) or through (non-gravitational) dark matter self-interactions (e.g. Spergel & Steinhardt, 2000).

Mashchenko et al. (2006) argued that cyclic star formation bursts within the centres of dark matter halos could provide the necessary energy to re-shape the dark matter cusp into a dark matter core. In this model, feedback from type II supernovae (SNe) periodically drives bulk gas motions in the star forming regions in the central kpc of dwarf galaxies. Since gas can dominate the central gravitational field, these bulk motions can significantly perturb the central gravitational potential on timescales comparable to dark matter orbital times leading to an efficient transfer of kinetic energy to the central dark matter distribution and the formation of a significant dark matter core. A notable feature of the Mashchenko et al. (2006) framework was that the gas need not be expelled or even pushed very far outside the core-forming region (as opposed to the impulsive blow-out scheme e.g. Navarro et al., 1996a; Read & Gilmore, 2005). Pontzen & Governato (2012) gave an analytical description of the process.

The mechanism was first verified in a cosmological simulation by Mashchenko et al. (2008). A required feature for simulations to flatten cusps is realistically clustered star formation so as to ensure a star formation history that significantly fluctuates in both space and time. Several simulations since have reproduced these results in a range of galaxies (e.g. Governato et al., 2010, 2012; Zolotov et al., 2012; Teyssier et al., 2013; Madau et al., 2014, see Pontzen & Governato 2014). The process also has consequences for other collisionless components such as stars and star clusters. Centrally concentrated populations (such as younger stars) are pushed outward over time, leading to older populations having larger orbits on average. This results in a broad match to observations of the stellar content of dwarf galaxies (e.g. Maxwell et al., 2012; Teyssier et al., 2013; Governato et al., 2014). It also has interesting consequences for multiple populations in galactic globular clusters (Maxwell et al., 2014).

Peñarrubia et al. (2012) suggested that SNe alone would have difficulty providing the energy required to form dark matter cores given the average stellar masses of dwarf galaxies. They employed a direct analytical estimate of the energy difference between a cored and a cuspy dark matter halo of the same total mass. Though there are other sources of energy, such as stellar winds and the ionizing flux from young stars (e.g. Leitherer et al., 1999), it is not clear that this added energy would be sufficient to remove the discrepancy or couple as well as SNe. However, the Peñarrubia et al. (2012) results are difficult to reconcile with the core forming simulations which typically employ feedback only from SNe (and with realistic efficiencies).

In this work we re-examine the energy requirements and show that the formation of dark matter cores is energetically plausible in a $\Lambda$CDM cosmology. The layout of the paper is as follows. §2.2 deals with the ambiguity inherent in the definition of a core size, and argues for a new, general way to define the core radius. In §2.3 we discuss the energy required to form dark matter cores in halos that were initially cuspy using assumptions that are more consistent with our understanding of how the process operates. In §2.4 we show predictions for core sizes in dark matter halos and examine the implications for observed systems such as Fornax.

## 2.2 Consistent Definition of Core Size

Many 'observed' cores in dwarf galaxies are inferred from the rotation profiles of the stars and gas by finding the best-fit dark-matter density model (e.g. Flores & Primack, 1994; Burkert, 1995; Kuzio de Naray et al., 2006; Gilmore et al., 2007; Kuzio de Naray et al., 2008; Oh et al., 2011). Commonly, one would use either a cored isothermal sphere, whose density profile goes as $r^{-2}$ at large radii, or that proposed by Burkert (1995) where the density goes as $r^{-3}$ at large radii,

$$\rho(r) \propto \frac{1}{\left(1 + (\frac{r}{r_{\rm s}})\right)\left(1 + (\frac{r}{r_{\rm s}})^2\right)}. \tag{2.1}$$

Both satisfy the requirement that the density profile transitions to a flat core within a scale radius. Without probing the rotation profile to large radii it is difficult to determine which density profile is the best fit. The cored isothermal profile predicts a constant velocity at large radii while the Burkert (1995) profile looks like the standard galaxy rotation curve (e.g. Rubin et al., 1978). However, the common practice of defining the scale radius as the core size leads to large variations in core radii dependent on the chosen functional form.

To avoid this ambiguity, we define the core radius as *the radius, $r_{\rm c}$, at which the logarithmic slope of the density profile satisfies*:

$$\frac{{\rm d}\ln\rho}{{\rm d}\ln{\rm r}} = -\frac{1}{2}.$$

We will use this definition from now on when referring to the core size. It is consistent with the density profile slopes found in simulations of dwarf galaxies (e.g. Mashchenko et al., 2008; Governato et al., 2010; Teyssier et al., 2013) and with the mass profile slopes observed in local group dwarfs (e.g. Walker & Peñarrubia, 2011; Amorisco et al., 2013; Adams et al., 2014). Furthermore, the simulated galaxies always transition to a density profile with a strongly negative slope ($\mathrm{d}\ln\rho/\mathrm{d}\ln\mathrm{r} \simeq -3$) beyond a few kpc where the effects of baryonic feedback are limited. This definition of the core radius lessens the reliance on an assumed dark matter density distribution, and it can be determined directly from the velocity profile. It is also straightforward to relate $r_\mathrm{s}$ to $r_\mathrm{c}$ for a given density profile.

To demonstrate the robustness of our new core definition, and to illustrate the ambiguity with using the scale radius, we show in Figure 2.1 the rotational velocity profile for the Low Surface Brightness (LSB) galaxy NGC 959 from Kuzio de Naray et al. (2008). These authors assumed a cored isothermal density profile, and the best fit of this profile to the data is shown as the solid line. Although it is perfectly sufficient to match the profile in the inner 1–2 kpc, it does not roll over sufficiently to match the slope in the outer part of a cosmological halo. We have also fit three other density profiles. The first, shown as the dotted line in the figure, is (e.g. Widrow, 2000, 'Fixed' in the figure):

$$\rho(r) \propto \frac{1}{\left(1 + (\frac{r}{r_\mathrm{s}})^{\alpha}\right)^{3/\alpha}}. \tag{2.2}$$

The second, shown as the dashed line, is a pseudo-isothermal profile, where we let the power index vary:

$$\rho(r) \propto \frac{1}{1 + (\frac{r}{r_\mathrm{s}})^{\delta}}. \tag{2.3}$$

Lastly, we show the Burkert (1995, Eqn. 2.1) profile as the dash-dot line.

The differences between the three rotation profile fits are only evident at radii past the furthest observable point, where the predicted rotation velocity rolls over. We have also done this for the eight other LSBs from Kuzio de Naray et al. (2008) (see Appendix), and the resulting scale radii and core radii are shown in Table 2.1. It is evident that velocity rotation data alone are not enough to distinguish the best fit dark matter density profile for the core. Furthermore, each fit requires a different scale radius, the traditional definition of the core size. However, using $\mathrm{d}\ln\rho/\mathrm{d}\ln\mathrm{r}$ to define the core radius leads to consistent values for the four density profiles for most of the LSBs.

There are some LSBs that do not show consistent $r_\mathrm{c}$ values, particularly UGC 4325 and DDO 64. In the constant density core the velocity profile scales linearly with radius, and rolls over to a constant or decreasing slope as the density profile begins to fall. For galaxies that only have data points within the constant density core, a fitting algorithm is only able to place lower bounds on $r_\mathrm{c}$ and is certainly not able to constrain the parameters of a non-linear density function.

## 2.3 The Core Formation Energy Budget

In this section we estimate the energy required to build a core in an initially ‘cuspy’ density profile. We assume that each cuspy halo begins with an ‘NFW’ profile (Navarro et al., 1995, 1996b, 1997). We can estimate the energy as the difference between the work required to form the cusp and the work required to form the core, assuming the halos are virialized in both cases (Peñarrubia et al., 2012):

$$\Delta E = \frac{W_\mathrm{c} - W_\mathrm{h}}{2}, \tag{2.4}$$

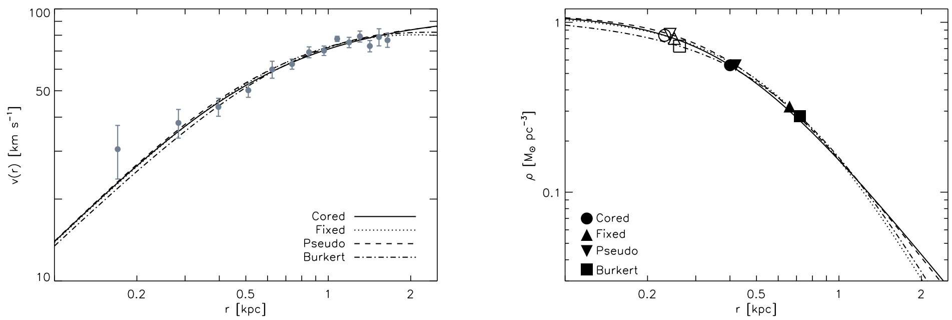


Figure 2.1: *LEFT*: The velocity profile of the LSB NGC 959 from Kuzio de Naray et al. (2008), with the best fit 'zero disk' cored isothermal profile shown as the solid line. The dotted line shows the best fit using Equation (2.2), the dashed line shows Equation (2.3) and the dash-dot line shows the best fit using the Burkert (1995) profile (Eqn. 2.1). For many of these halos, differences between the cored profiles are only evident at radii well outside the available observations. *RIGHT*: The dark matter density profiles derived from the best fit velocity profiles. For the same observed dwarf galaxy four different scale radii, the traditional definition of the core size, can be derived. The filled symbols show $r_s$ for each of the four profiles, while the open symbols show $r_c$, where $\mathrm{d}\ln\rho/\mathrm{d}\ln\mathrm{r} = -1/2$.

Table 2.1. Best fit parameters.

| | Cored[a] | | | Pseudo | | | Fixed | | | Burkert | |
|---|---|---|---|---|---|---|---|---|---|---|---|
| Galaxy | $\delta$ | $r_s$ | $r_c$ | $\delta$ | $r_s$ | $r_c$ | $\alpha$ | $r_s$ | $r_c$ | $r_s$ | $r_c$ |
| UGC 4325 | 2 | 4.1 | 2.37 | 1.26 | 9.92 | 7.12 | 1.66 | 9.60 | 3.64 | 9.97 | 3.62 |
| DDO 64 | 2 | 3.3 | 1.91 | 9.97 | 2.63 | 1.96 | 9.97 | 2.21 | 1.88 | 9.91 | 3.60 |
| F583-1 | 2 | 2.5 | 1.44 | 1.93 | 2.48 | 1.44 | 1.81 | 3.67 | 1.51 | 4.46 | 1.62 |
| NGC 7137 | 2 | 0.6 | 0.35 | 1.97 | 0.60 | 0.35 | 1.44 | 1.12 | 0.37 | 1.09 | 0.40 |
| UGC 11820 | 2 | 1.1 | 0.64 | 3.78 | 1.14 | 0.69 | 9.27 | 0.89 | 0.75 | 2.10 | 0.76 |
| UGC 128 | 2 | 2.3 | 1.33 | 1.00 | 1.41 | 1.41 | 1.00 | 7.69 | 1.54 | 4.63 | 1.68 |
| UGC 191 | 2 | 1.7 | 0.98 | 1.22 | 2.00 | 1.48 | 1.06 | 6.72 | 1.47 | 3.45 | 1.25 |
| UGC 1551 | 2 | 1.3 | 0.75 | 1.00 | 0.92 | 0.92 | 1.00 | 4.14 | 0.83 | 2.26 | 0.82 |
| NGC 959 | 2 | 0.4 | 0.23 | 2.09 | 0.42 | 0.24 | 1.66 | 0.66 | 0.25 | 0.72 | 0.26 |

[a]Kuzio de Naray et al. (2008).

Note. — These parameters represent the best fitting density profiles required to match the central core density out to the edge of the rotation profile data of Kuzio de Naray et al. (2008). All radii are in kpc. The scale sizes for the four different profiles, the traditional definition of the core size, vary widely despite having the same inner central density and matching the velocity data. The new definition of core size is much more consistent among profiles.

where $W_{\rm h}$ and $W_{\rm c}$ are the cusp and core potential energies, respectively. $\Delta E > 0$ implies the cusped dark matter halo had to gain energy to redistribute mass to form a core. If the simplifying assumption is made that both halos are spherically symmetric, we can write the potential energy integral as (Binney & Tremaine, 2008):

$$W = -4\pi G \int_0^\infty r\rho(r)M(r)\,\mathrm{dr}. \tag{2.5}$$

For a density profile that goes as $\rho \propto r^{-\beta}$ at large $r$, the integral converges for $\beta > 5/2$; all of the cored profiles considered (if $\delta > 5/2$ in Eqn. 2.3) and the NFW profile lead to well defined values for $W$.

Taking the upper limit in Equation (2.5) to infinity leads to a very large estimate for the energy (quite apart from the ambiguity of embedding the halo in the cosmic background) and is not appropriate given that we are considering *re-distributing* mass within an existing halo. Peñarrubia et al. (2012) chose the halo virial radius $r_{\rm s}$ as the upper limit for the potential energy integral, and normalised the mass of their chosen core density profile,

$$\rho(r) = \frac{\rho_{\rm o} r_s^3}{(r_c + r)(r_s + r)^2}, \tag{2.6}$$

to that of their initial NFW halo at $r_{\rm h}$. However, simply normalising both halos to have the same mass at $r_{\rm s}$ does not remove the requirement that Equation (2.5) be carried to infinity. In order for the potential energy integral to be valid with a finite upper limit $r_{\rm m}$, the density *and* mass profiles for both halos must match at that radius. The choice of Peñarrubia et al. (2012) to match the mass at $r_{\rm s}$ and to truncate the integral for $W$ at that radius builds in an implicit discontinuity in the density at that radius that is not physically well motivated. Furthermore, moving the cusp mass to near the virial radius of the halo leads to a core formation energy budget from Equations (2.5) and (2.4) which will be significantly overestimated compared with that for match radii, $r_{\rm m} \ll r_{\rm h}$.

The motivation for constraining the mass and density profiles of the pre- and post-core halos outside $r_{\rm m}$ to be the same is simply that we expect that strong coupling of star formation feedback to dark matter is only effective in, and only modifies, the central parts of the halo. The outer parts of the halo will remain largely untouched and reflect the collisionless formation process. This picture is supported by simulations (e.g. Mashchenko et al., 2006, 2008; Governato et al., 2010; Pontzen & Governato, 2012; Teyssier et al., 2013; Madau et al., 2014). Previous simulations (Mashchenko et al., 2008; Madau et al., 2014) suggest that for a $\sim 10^{10}$ $\mathrm{M}_{\odot}$ halo $r_{\rm m}$ is about 2–3 times the core radius.

Our method proceeds as follows:

- Since we do not have any robust predictions of what the core profile should be, we adopt Equation (2.3) as the density profile when computing $W_{\rm c}$. (We have verified that using a different density profile, such as Equation (2.1) or Equation (2.2), does not change our results.)

- We use the relations given by Macciò et al. (2007) and Bryan & Norman (1998) to set the NFW profile at redshift zero as a function of virial halo mass, $M_{\rm h}$ (see Peñarrubia et al., 2012). We then have $\rho(r_{\rm m})$ and $M(r_{\rm m})$ as functions of $M_{\rm h}$.

- We find the set of parameters $\rho_{\rm o}$, $\delta$, and $r_{\rm c}$ for the cored density profile that *simultaneously* satisfy $\rho(r_{\rm m})$ and $M(r_{\rm m})$ from the previous step.

- We set $r_{\rm m} = 3r_{\rm c}$, where $r_{\rm c}$ is given by our new definition. Figure 2.2 illus-

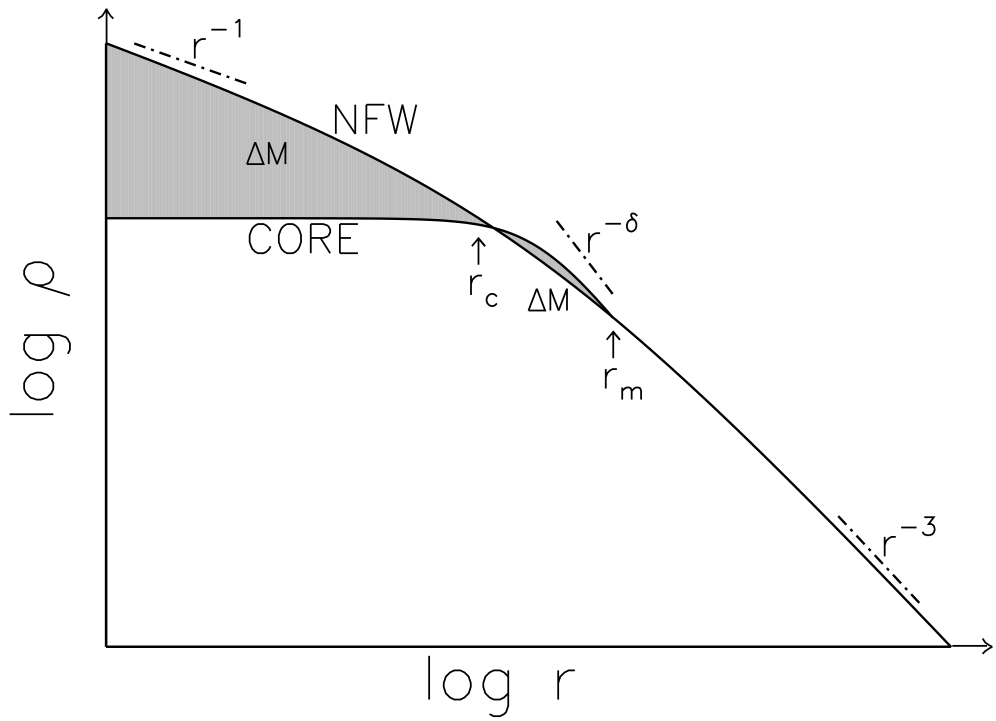


Figure 2.2: A pictorial representation of our procedure to match both density and mass of the core and cusp density profiles at $r_\mathrm{m}$. The leftmost shaded region shows the amount of mass that must be redistributed from the cusp to larger radii (up to $r_\mathrm{m}$) in the cored profile. Not having to redistribute mass to larger radii near the virial radius explains why our predictions for the energy cost of core formation are significantly below previous estimates. It is purely coincidental that in this illustration the core radius, $r_\mathrm{c}$, is close to the radius at which the two density profiles first cross.

trates the profile and mass matching.

- We compute the potential energy difference in Eqn (2.4).

The preceding steps give $\Delta E$ in terms of $r_\mathrm{c}$ and $M_\mathrm{h}$.

## 2.4 Results

In Figure 2.3 we show our calculation for the amount of energy required to turn a dark matter cusp into a core as a function of halo mass. Since we may write approximately:

$$W_{\rm c} \sim \frac{GM(<r_{\rm m})^2}{r_{\rm m}}, \tag{2.7}$$

for the cored profile, we see, as expected, that the parameter that most influences the energy required to convert a cusp into a core is $r_{\rm m} \propto r_{\rm c}$; a larger core requires more mass at larger radii and thus more energy to redistribute it from the cusp. The black line shows that $\Delta E$ scales as $M_{\rm h}^{1.6}$ if $r_{\rm m}$ is instead allowed to scale[1] with halo mass, and lies within the range of solutions calculated by Peñarrubia et al. (2012), shown here by the gray shaded region. However, since we force *both* the density and mass to match the outer NFW-like halo at $r_{\rm m}$, the energy required to make an appreciable core ($\sim 1$ kpc) is greatly reduced. This is shown in Figure 2.3 for core sizes between 0.1–8 kpc. Varying the ratio $r_{\rm m}/r_{\rm c}$, currently set to 3, merely shifts the $\Delta E$ curves vertically.

The significance of our new calculations can be seen by comparing to the stellar-halo mass relation ($M_{\rm s}$-$M_{\rm h}$). In Figure 2.3 we plot $M_{\rm s}$-$M_{\rm h}$ relations from Kravtsov (2010) (dashed), Behroozi et al. (2010) (dotted), and Moster et al. (2010) (dash-dot) at $z = 0$. We have converted $M_{\rm s}$ to total SNe energy using a Kroupa (2001) IMF, assuming that every star above 8 $\rm M_\odot$ contributes $10^{51}$ ergs to the energy budget. Our results show that *there is no conflict between the amount of energy available to form a dark matter core and the $\Lambda$CDM framework*, regardless of halo mass.

In reality, not all of the SNe energy will couple to the cusp dark matter

[1] In other words, as a fixed fraction of $r_{\rm s}$ (here 1/6).

through the induced perturbations to the gravitational potential. This inefficiency can be proxied in the $M_{\rm s}$-$M_{\rm h}$ relations shown in Figure 2.3 by scaling them by some coupling efficiency factor $\epsilon$ (for example, the 40% value used by Peñarrubia et al., 2012). Only for $\epsilon \lesssim 0.01\%$ would there be no possibility of creating a core larger than 250 pc in the $10^9$–$10^{10}$ $M_\odot$halo range. We are thus forced to conclude that most, if not all, dwarf galaxies should host dark matter cores if their central star formation rate was high enough to build $10^3$–$10^4$ $M_\odot$ in stars.

Our calculations suggest that limiting $r_{\rm m}/r_{\rm c}$ to only 2–3 reduces the energy scaling as a function of halo mass for a given core size, thereby making them easier to form in a cosmological setting. As shown in Figure 2.3 the scaling is much weaker when both $r_{\rm c}$ and $r_{\rm m}$ are fixed. For example, $\Delta E$ scales as $M_{\rm h}^{0.7}$ in the $10^9$–$10^{10}$ $M_\odot$ halo mass range for a 1 kpc core, but only as $M_{\rm h}^{0.3}$ in the same range when $r_{\rm c}$ is fixed to be 100 pc. This is expected given that the mass interior to $r_{\rm m}$ depends on the halo concentration, and in the functional form we adopted the concentration is inversely proportional to $M_{\rm h}$ (Macciò et al., 2007). Thus, the the ability to form a core of size $r_{\rm c}$ whose density and mass are constrained at $r_{\rm m}$ is independent of the actual halo mass; instead, it is the mass distribution interior to $r_{\rm m}$ that affects the energy requirement.

Our results are insensitive to the redshift dependence of halo parameters such as $M_{\rm h}$, $r_{\rm s}$, and $r_{\rm s}$. These parameters merely set $M(< r_{\rm m})$ as a function of $r_{\rm m}$, which can be considered redshift independent. The ability for a given halo to form a core will depend on the coupling between the depth of the central halo potential and the star formation rate which limits the amount of available feedback energy. The bursty star formation at the centres of dwarf galaxies should be able to drive $\epsilon$ high enough to form a sizeable core (Maxwell et al., 2012) at high redshift (Mashchenko et al., 2008; Amorisco et al., 2014; Madau et al., 2014). However, low mass halos

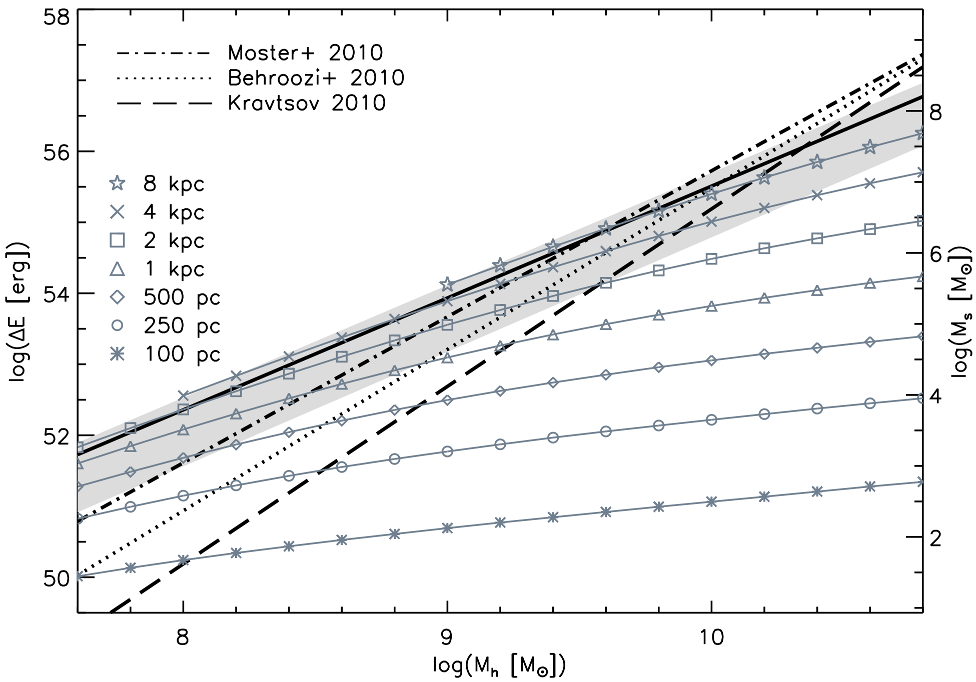


Figure 2.3: The estimate of the amount of energy $\Delta E$ required to convert a dark matter cusp into a core. The solid lines with symbols show the energy required to form a core of a given fixed size using the pseudo-isothermal density profile (see text). The solid black line shows how $\Delta E$ scales with $M_{\rm h}$ if $r_{\rm m}$ is allowed to scale as a fixed fraction of $r_{\rm s}$. The grey area corresponds to the energy estimate of Peñarrubia et al. (2012). The dotted, dashed, and dot-dashed lines correspond to the $M_{\rm s}$-$M_{\rm h}$ relations of Behroozi et al. (2010), Kravtsov (2010), and Moster et al. (2010) respectively, assuming a Kroupa (2001) IMF. The right axis shows the stellar mass corresponding to $\Delta E$ assuming 100% efficiency.

may not be able to form cores if their galactic potential is shallow enough that each burst of star formation results in completely efficient gas expulsion (e.g. Navarro et al., 1996a; Read & Gilmore, 2005; Shen et al., 2013; Madau et al., 2014).

## 2.5 Discussion

In the previous section we showed that stellar feedback, of which we have only considered SNe, can provide enough energy to the dense star forming gas in the centres of dwarf galaxies to transform the dark matter cusps predicted by numerical experiments to the flattened dark matter cores inferred from observations (e.g. Mashchenko et al., 2008; Pontzen & Governato, 2012; Maxwell et al., 2012). This is due to our adoption of a more robust mass normalisation criterion than previous work (e.g. Peñarrubia et al., 2012). The most efficienct injection of star formation feedback energy will occur at the deepest point in the galactic potential, which implies a physical limit to the radius to which cusp dark matter can be redistributed. In our calculations, we have parameterized this limit as the radius $r_{\rm m}$, beyond which the dark matter mass and density profiles are unchanged, being set by the collisionless merging process. Our results suggest significant dark matter cores can be formed with less than 1% of the total SNe energy available over the star forming history of a typical dwarf galaxy.

So far we have been concerned with whether a dark matter core can form in an initially cuspy halo due to star formation feedback. Our new calculations allow us to ask a more physically motivated question: what is the typical core size for a given halo mass? In Figure 2.4 we show the predicted core size as a function of halo mass using the three $M_{\rm s}$-$M_{\rm h}$ relations shown in Figure 2.3. Although Figure 2.4 reinforces our main conclusion that dark matter cores can form from cusps in even the smallest dwarf galaxy halos, it also emphasizes the uncertainty in trying to make detailed predictions. The variation in the low mass slope of the $M_{\rm s}$-$M_{\rm h}$ relation between the Moster et al. (2010), Behroozi et al. (2010), and Kravtsov (2010) results corresponds directly to a factor of 2–4 variation in predicted $r_{\rm c}$ as a function

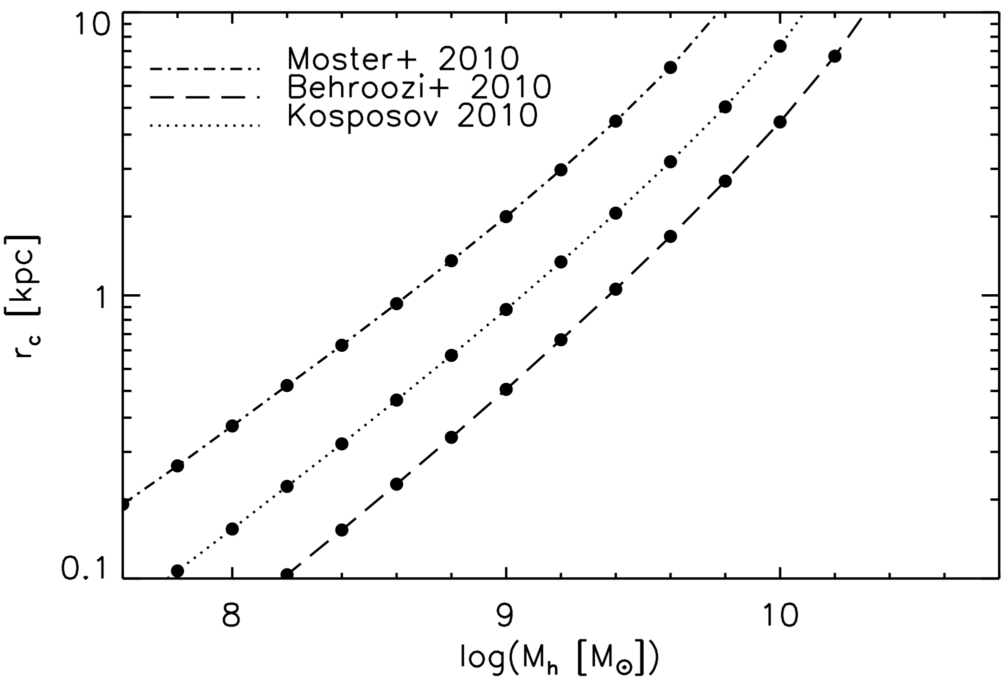


Figure 2.4: The predicted core size as a function of halo mass using the three $M_{\rm s}$-$M_{\rm h}$ relations discussed in this paper. It is extremely difficult to compare these predictions to observed dark matter cores in local group dwarf galaxies given the uncertainties in the relations, and the difficulty in determining $M_{\rm h}$ for individual galaxies.

of halo mass. Furthermore, these relations only give the average stellar mass as a function of halo mass.

Figure 2.4 is further complicated because we have not yet considered the efficiency with which the energy from stellar feedback is transferred to dark matter particle orbits. The coupling efficiency will likely vary in time with changing conditions in the centre of the halo, and will depend on the star formation rate, gas accretion rate, gas heating rate, and the dark matter particle orbits; the value of $\epsilon$ used in Peñarrubia et al. (2012) is merely a time-averaged value over the dwarf galaxy star formation and gas accretion histories. Finally, our results show that the energy required to form the core, $\Delta E$, has only a weak dependence on $M_{\rm h}$ for a given $r_{\rm c}$.

If, indeed, our ansatz that matter redistribution happens only within $r_{\rm m}$ is correct, it is more appropriate to ignore $M_{\rm h}$ altogether when comparing core sizes between dwarf galaxies. Many observations of dwarf galaxies in the local universe can only measure dynamical masses out to a few kpc (e.g. Dalcanton et al., 2009; Oh et al., 2011; Kuzio de Naray et al., 2006, 2008; McConnachie, 2012) and so cannot accurately determine the halo virial mass. This leads us to Figure 2.5 where we have plotted the range of core sizes as a function of stellar mass required to produce a core of that size, *without* adopting any efficiency in dark matter core formation. Each curve represents the track in $r_{\rm c}$-$M_{\rm s}$ space for each halo mass, and is determined by the relations between $M_{\rm h}$, $r_{\rm s}$, and $r_{\rm s}$ (or concentration parameter). The endpoints of each curve represent the upper and lower limits that we arbitrarily imposed when computing the energy requirements from Equation (2.5). Our upper bound was set at $r_{\rm c} \leq r_{\rm h}/6$, a conservative upper limit given the relatively small stellar profiles of dwarf galaxies.

The shape of the curve is consistent with one of the arguments of Peñarrubia et al. (2012) that the largest energy requirement comes from transforming the central cusp into a core. Further scouring of the core by reducing the central density and increasing the core size requires significantly less energy. Thus, for a given halo mass the predicted $r_{\rm c}$ vertically asymptotes as a function of $M_{\rm s}$. This same behaviour was found in recent simulations of dwarf galaxies (Shen et al., 2013; Madau et al., 2014).

In this figure, the efficiency $\epsilon$ is equivalent to sliding a given dwarf galaxy along the $M_{\rm s}$ axis. To illustrate this, we show the local group dwarf Fornax, whose stellar mass was taken from McConnachie (2012) and whose dark matter core size

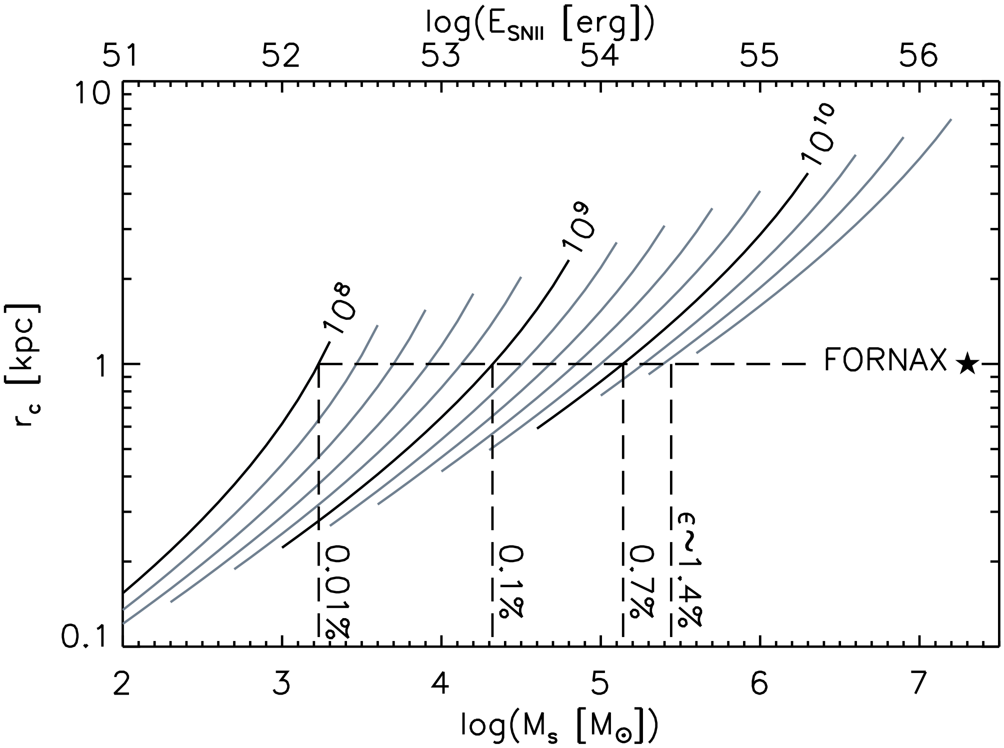


Figure 2.5: The predicted dark matter core *as a function of stellar mass*. The grey lines show the energy curve in $r_\mathrm{c}$-$M_\mathrm{s}$ space for a given $M_\mathrm{h}$. The top axis shows our assumed conversion from $M_\mathrm{s}$ to SNe energy. For clarity, we have highlighted the curves for halos of $10^8\,\mathrm{M}_\odot$, $10^9\,\mathrm{M}_\odot$, and $10^{10}\,\mathrm{M}_\odot$. The star shows the estimated stellar mass of Fornax from McConnachie (2012) with the dark matter core size estimated by Amorisco et al. (2013). The efficiency $\epsilon$ to which the SNe feedback couples to the creation of a dark matter core can be estimated by sliding the Fornax data point to the left.

was measured by Amorisco et al. (2013). Fornax lies significantly below the predicted core size for its stellar mass, but is consistent with our core predictions if only a few per cent of the total SNe budget contributed to the formation of the dark matter core in the host halo. Fornax's host halo could range anywhere from $10^8$–$10^{10}\,\mathrm{M}_\odot$ while $\epsilon$ could range anywhere from 0.01–1%.

## 2.6 Conclusions

In this paper we have estimated the energy requirement for supernovae to form dark matter cores in their host halos. By adopting a radius $r_{\rm m}$ at which both the density and mass profiles of the cored dark matter halo and the original cusped halo match, we find that the amount of energy required is significantly reduced from the estimate of Peñarrubia et al. (2012) without having to require cores to form only at high redshift (e.g. Amorisco et al., 2014). Our results suggest that dark matter cores are present in most, if not all, dark matter halos that experienced clustered star formation within their centres (Maxwell et al., 2012). This alleviates another problem pointed out by Peñarrubia et al.: the mixing of phase space densities for systems of collisionless particles was shown by Dehnen (2005) to tend to preserve the steepest density cusp in the merger. If many of the halos merging in the collisionless mass assembly process are already cored, the dark matter density profile of the merger remnant should be cored as well. Even if the core is destroyed via the accretion of a dark matter cusp, subsequent star formation feedback should be enough to destroy the dark matter cusp in a short time[2].

By relieving the tension between $\Lambda$CDM and the presence of cores in dwarf galaxies, we can now begin to make firm predictions of the sizes of dark matter cores as a function of stellar mass (Figure 2.5). For example, simulations of dark matter core formation in dwarf galaxies can provide a novel benchmark for the efficiency and energy output of star formation prescriptions, especially as observations of local dwarfs improve (e.g. Kuzio de Naray et al., 2008; Dalcanton et al., 2009). It is also important to note that we have neglected all other forms of star formation feedback (e.g. Hopkins et al., 2011, 2013; Shen et al., 2010; Agertz et al., 2013;

[2]The work of Mashchenko et al. (2008), for example, showed that a core can form in $\sim 100$ Myr.

Keller et al., 2014), but these extra sources of energy can simply be proxied by $\epsilon$, the efficiency with which the energy is transferred to the dark matter. Since many of the above studies have either focused on the small scale evolution of single molecular clouds or a Milky-Way type galaxy, dwarf galaxies still represent an attractive laboratory within which to study structure formation models in a cosmological context with acceptable physical resolution.

The authors wish to thank NSERC for support and R. Kuzio De Naray for providing the observed rotation profile data.

## Appendix

Figure 2.6 repeats the analysis shown in Figure 2.1 for all nine Low Surface Brightness galaxies observed by Kuzio de Naray et al. (2008).

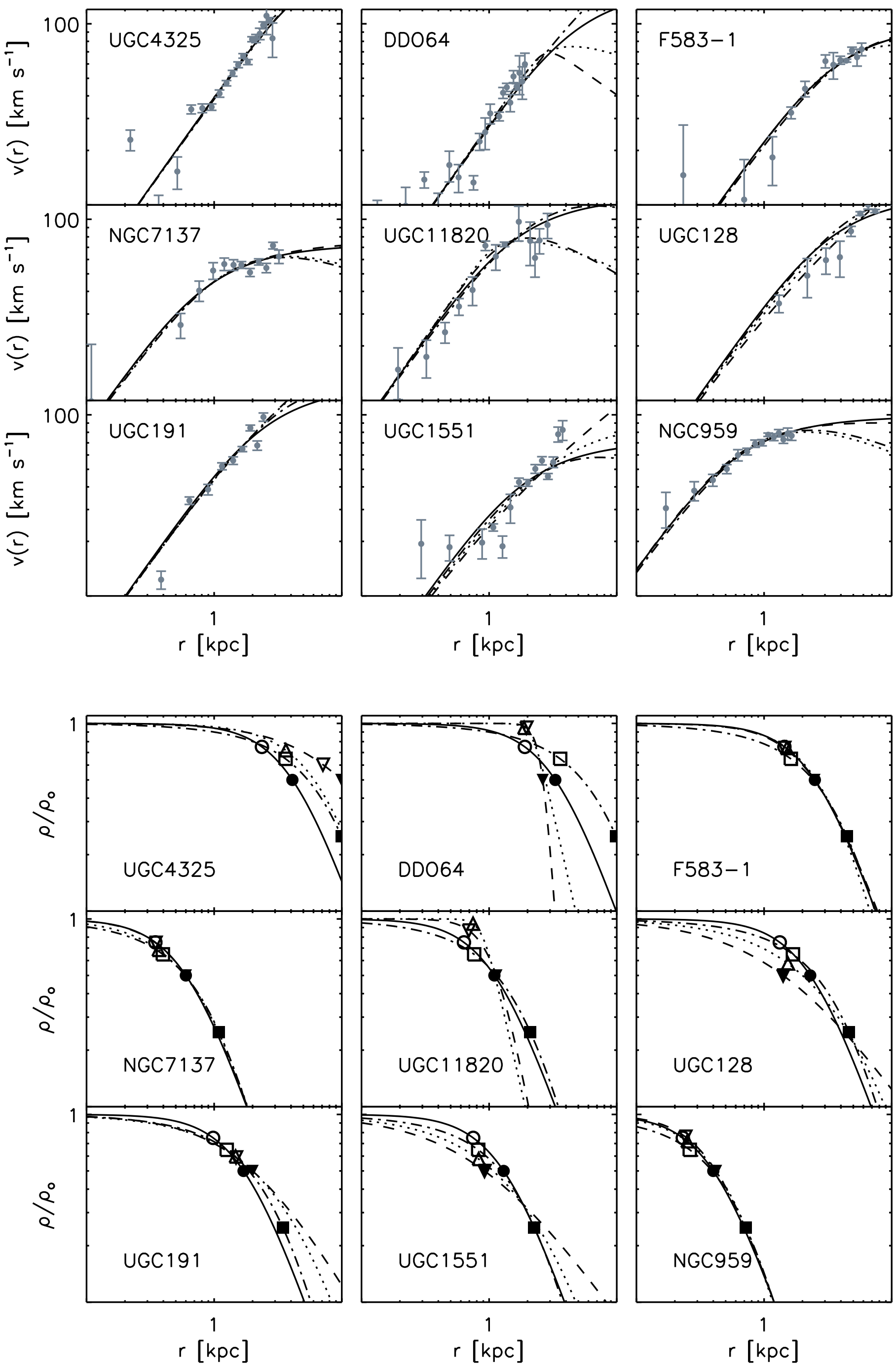


Figure 2.6: The velocity and density profiles for all of the Kuzio de Naray et al. (2008) LSBs. Line styles and symbols are the same as in Figure 2.1.

# Bibliography


Adams, J. J., Simon, J. D., Fabricius, M. H., et al. 2014, ApJ, 789, 63

Agertz, O., Kravtsov, A. V., Leitner, S. N., & Gnedin, N. Y. 2013, ApJ, 770, 25

Amorisco, N. C., Agnello, A., & Evans, N. W. 2013, MNRAS, 429, L89

Amorisco, N. C., Zavala, J., & de Boer, T. J. L. 2014, ApJL, 782, L39

Behroozi, P. S., Conroy, C., & Wechsler, R. H. 2010, ApJ, 717, 379

Binney, J., & Tremaine, S. 2008, Galactic Dynamics: Second Edition (Princeton University Press)

Bosma, A. 1981, AJ, 86, 1825

Bryan, G. L., & Norman, M. L. 1998, ApJ, 495, 80

Bullock, J. S., Kolatt, T. S., Sigad, Y., et al. 2001, MNRAS, 321, 559

Burkert, A. 1995, ApJL, 447, L25

Côté, S., Carignan, C., & Freeman, K. C. 2000, AJ, 120, 3027

Dalcanton, J. J., Williams, B. F., Seth, A. C., et al. 2009, ApJS, 183, 67

Dehnen, W. 2005, MNRAS, 360, 892

Dubinski, J., Berentzen, I., & Shlosman, I. 2009, ApJ, 697, 293

Dubinski, J., & Carlberg, R. G. 1991, ApJ, 378, 496

El-Zant, A., Shlosman, I., & Hoffman, Y. 2001, ApJ, 560, 636

Flores, R. A., & Primack, J. R. 1994, ApJL, 427, L1

Gilmore, G., Wilkinson, M. I., Wyse, R. F. G., et al. 2007, ApJ, 663, 948

Governato, F., Brook, C., Mayer, L., et al. 2010, Nature, 463, 203

Governato, F., Zolotov, A., Pontzen, A., et al. 2012, MNRAS, 422, 1231

Governato, F., Weisz, D., Pontzen, A., et al. 2014, arXiv:1407.0022

Hogan, C. J., & Dalcanton, J. J. 2000, PhRvD, 62, 063511

Hopkins, P. F., Keres, D., Onorbe, J., et al. 2013, arXiv:1311.2073

Hopkins, P. F., Quataert, E., & Murray, N. 2011, MNRAS, 417, 950

Jardel, J. R., & Sellwood, J. A. 2009, ApJ, 691, 1300

Keller, B. W., Wadsley, J., Benincasa, S. M., & Couchman, H. M. P. 2014, MNRAS, 442, 3013

Klypin, A., Kravtsov, A. V., Bullock, J. S., & Primack, J. R. 2001, ApJ, 554, 903

Kravtsov, A. 2010, AdAst, 2010

Kroupa, P. 2001, MNRAS, 322, 231

Kuzio de Naray, R., McGaugh, S. S., & de Blok, W. J. G. 2008, ApJ, 676, 920

Kuzio de Naray, R., McGaugh, S. S., de Blok, W. J. G., & Bosma, A. 2006, ApJS, 165, 461

Leitherer, C., Schaerer, D., Goldader, J. D., et al. 1999, ApJS, 123, 3

Macciò, A. V., Dutton, A. A., van den Bosch, F. C., et al. 2007, MNRAS, 378, 55

Madau, P., Shen, S., & Governato, F. 2014, ApJL, 789, L17

Mashchenko, S., Couchman, H. M. P., & Wadsley, J. 2006, Nature, 442, 539

Mashchenko, S., Wadsley, J., & Couchman, H. M. P. 2008, Science, 319, 174

Maxwell, A. J., Wadsley, J., Couchman, H. M. P., & Mashchenko, S. 2012, ApJL, 755, L35

Maxwell, A. J., Wadsley, J., Couchman, H. M. P., & Sills, A. 2014, MNRAS, 439, 2043

McConnachie, A. W. 2012, AJ, 144, 4

Moore, B. 1994, Nature, 370, 629

Moster, B. P., Somerville, R. S., Maulbetsch, C., et al. 2010, ApJ, 710, 903

Navarro, J. F., Eke, V. R., & Frenk, C. S. 1996a, MNRAS, 283, L72

Navarro, J. F., Frenk, C. S., & White, S. D. M. 1995, MNRAS, 275, 720

—. 1996b, ApJ, 462, 563

—. 1997, ApJ, 490, 493

Oh, S.-H., de Blok, W. J. G., Brinks, E., Walter, F., & Kennicutt, Jr., R. C. 2011, AJ, 141, 193

Peñarrubia, J., Pontzen, A., Walker, M. G., & Koposov, S. E. 2012, ApJL, 759, L42

Pontzen, A., & Governato, F. 2012, MNRAS, 421, 3464

—. 2014, Nature, 506, 171

Read, J. I., & Gilmore, G. 2005, MNRAS, 356, 107

Rubin, V. C., Ford, W. K. J., & . Thonnard, N. 1980, ApJ, 238, 471

Rubin, V. C., Thonnard, N., & Ford, Jr., W. K. 1978, ApJL, 225, L107

Sellwood, J. A. 2003, ApJ, 587, 638

Shen, S., Madau, P., Conroy, C., Governato, F., & Mayer, L. 2013, arXiv:1308.4131

Shen, S., Wadsley, J., & Stinson, G. 2010, MNRAS, 407, 1581

Spergel, D. N., & Steinhardt, P. J. 2000, PhRvL, 84, 3760

Stadel, J., Potter, D., Moore, B., et al. 2009, MNRAS, 398, L21

Tasitsiomi, A. 2003, IJMPD, 12, 1157

Teyssier, R., Pontzen, A., Dubois, Y., & Read, J. I. 2013, MNRAS, 429, 3068

Walker, M. G., & Peñarrubia, J. 2011, ApJ, 742, 20

Weinberg, M. D., & Katz, N. 2002, ApJ, 580, 627

Widrow, L. M. 2000, ApJS, 131, 39

Zolotov, A., Brooks, A. M., Willman, B., et al. 2012, ApJ, 761, 71

Chapter 3

# Building the Stellar Halo Through Feedback in Dwarf Galaxies

Reprinted from Aaron J. Maxwell, James Wadsley, H. M. P. Couchman, and Sergey Mashchenko *2012*, THE ASTROPHYSICAL JOURNAL LETTERS, *Volume 755, Issue 2, pp. 35–39, DOI: 10.1088/2041-8205/755/2/L35.* ©*AAS.*

## 3.1 Introduction

Dwarf galaxies are the predominant star forming objects in the early universe and dwarf spheroidals, in particular, are fossil remnants of this era (Dekel & Silk, 1986). Normal star formation (post-Population III) occurs in the densest gas accumulating in the centres of galactic potential wells. In this case, we might expect dwarf spheroids to be simple, highly concentrated, star piles. In contrast, the stars in observed dwarfs are diffuse and many lack a conspicuous nucleus. Further, dwarfs at or above the luminosity of Fornax have their own globular cluster systems (Mateo, 1998). If these galaxies were the first objects large enough to have a high-pressure

ISM in their centres, capable of forming large clusters, we need to explain how such clusters could end up orbiting at substantial radii with a distribution similar to that of the overall light (Miller, 2009). Radial age and metallicity gradients are also observed (McConnachie, 2012), suggesting an outside-in formation scenario reminiscent of the “monolithic collapse” model (Eggen et al., 1962, hereafter ELS).

In this paper, we explore how features present in the old stellar populations of dwarf galaxies can occur naturally in contemporary cosmological models through star formation and feedback in these galaxies. Young dwarf galaxies have a high gas content and form stars vigorously. In prior work, Mashchenko et al. (2008) were able to show that stellar feedback in a simulated dwarf galaxy will drive bulk gas motions that couple gravitationally to all matter near the centre of the dwarf. As discussed in §3.2, this mechanism has been shown to act in actively star forming galaxies at a range of masses and is believed to be generic. The process pumps energy into the orbits of all material passing near the centre, transforming an initial dark matter cusp into a broad core, consistent with observations. Here we study the evolution of the stellar content, which is formed self-consistently in those simulations. Orbit pumping also operates on stars, the other key collisionless component of galaxies, to grow stellar spheroids from the inside out, as well as place massive star clusters on large radial orbits.

It is widely understood that the $\Lambda$CDM cosmology predicts the hierarchical assembly of galaxies: dwarf proto-galaxies interact and merge into larger galaxies, contrary to the ELS model. Searle & Zinn (1978) and Zinn (1980) refined this model by invoking a late in-fall of old stars that would contribute to both the stellar halo and its globular cluster population. Subsequent work has focused on reconciling this picture for the formation of the Galactic stellar halo with the standard hierarchical framework (for a recent review see Helmi, 2008). Chemical enrichment models combined with descriptions of a Milky Way (MW)-type merger history (e.g. Robertson et al., 2005; Bullock & Johnston, 2005; De Lucia & Helmi, 2008) and cosmological simulations of MW-type galaxies (e.g. Zolotov et al., 2010) can be made to match the abundance patterns of the stellar halo (e.g. Carollo et al., 2007, 2010; de Jong et al., 2010). A general conclusion is that dwarf progenitors play a major role in building the MW halo, owing to their high rates of star formation at early times and their ability to retain supernova-enriched gas.

However, MW-scale simulations poorly resolve dwarf galaxies which thus readily disintegrate and contribute their entire stellar contents to the halo. This conclusion is a direct consequence of low numerical resolution and is at odds with how star formation would be expected to occur in dwarfs. A closer understanding of star formation in dwarf galaxies is needed to establish how those stars are produced and how readily they can contribute to the observed Galactic stellar populations and their radial variations.

In §3.2 we discuss the stellar redistribution mechanism and how it operates. In §3.3 we explore the impact this has on the formation of the stellar spheroid in dwarfs including stellar systems such as globular clusters. We also discuss implications for dwarfs contributing their stars to the spheroids of larger galaxies.

## 3.2 Dynamical Impact of Stellar Feedback

Observations of the kinematics of the stellar and gaseous components of dwarf galaxies point to these systems having a cored density profile (e.g. Burkert, 1995; Côté et al., 2000; Gilmore et al., 2007; Oh et al., 2011, see de Blok (2010) for a recent review) in contrast to collisionless simulations of Cold Dark Matter (CDM) haloes which predict a central density cusp (e.g. Dubinski & Carlberg, 1991; Navarro et al., 1995; Bullock et al., 2001; Klypin et al., 2001; Stadel et al., 2009). Mashchenko et al. (2008) presented a solution to this long-standing challenge for the CDM cosmogony by correctly accounting for the the impact of stellar feedback. By feeding the energy generated by supernovae into the surrounding star-forming gas, they were able to generate fluctuations in the gravitational potential that pumped the dark matter orbits and removed the cusp. The effectiveness of dark matter orbit pumping due to stellar feedback has been confirmed in simulations by other workers, showing that it operates in dwarfs to the present day (Governato et al., 2010) and also affects larger galaxies up to Milky Way scales with sufficiently strong feedback (Macciò et al., 2012). In addition to operating in the SPH code used by Mashchenko et al. (2008), the mechanism has also been demonstrated using a grid code[1].

Two critical features allowed Mashchenko et al. (2008) to demonstrate the effect of stellar feedback on dark matter orbits in the dwarf galaxy: high resolution ($300\,\mathrm{M}_\odot$ per gas particle) and low temperature metal cooling (10–$8000\,\mathrm{K}$). The combination of these features allowed the formation of a cold, dense gas phase and permitted the use of a far more realistic minimum density for star formation, $\sim 100$ atoms cm$^{-3}$, comparable to molecular cloud densities. This was in sharp contrast to prior work where star formation occurred fairly uniformly throughout the ISM of simulated galaxies. As a result this was the first cosmological simulation to form numerically resolved star clusters up to $\sim 10^5\,\mathrm{M}_\odot$.

A direct result of clustered star formation is highly localized and episodic feedback that violently rearranges the gas in the inner regions of the dwarf galaxy. Since the gas dominates the mass in the star forming region, this results in a gravitational potential that varies on a timescale commensurate with orbital times. This

[1] R. Teyssier, priv. comm.

causes irreversible changes in the orbital energies of all matter passing near the star-forming centre of the dwarf. Whereas sharp changes in the potential impulsively modify all particle orbits (Pontzen & Governato, 2012), Mashchenko et al. (2006) showed that oscillating potentials with speeds closer to the typical particle velocity couple strongly and flatten the core more rapidly (their figure 2). For material that initially has a low velocity dispersion, such as dark matter within the cusp, this preferentially increases the orbital radius and redistributes the material into a smooth core as shown in Mashchenko et al. (2008) and other works. For the gaseous component, shocks dissipate this added velocity whereas dark matter and stars undergo a random walk in orbital energy.

We use the simulated dwarf of Mashchenko et al. (2008) to illustrate the process. We selected a period between redshifts 8–5 without major mergers so that the evolution is dominated by centralized star formation fueled by a consistent gas supply. Figure 3.1 shows several cycles of star formation, feedback upon the gas content and the response of the collisionless components. In this simulation, the majority of stars form within 100 pc, which we use as a radial size in which to measure the feedback effects. The centre is defined as the position of the 100 most bound particles. This choice biases towards gas-rich star-forming regions but gives very similar results to using a mass-weighted centre. The central 100 pc region is well resolved in space and mass.

In Figure 3.1a, the total star formation rate in units of $M_\odot\,yr^{-1}$ is shown for all stars formed within 100 pc. The star formation is highly episodic in this redshift range. Given that star formation is confined to a small central region, stellar feedback is very efficient at cutting off the supply of cold, dense gas that fuels the process. In the feedback model employed in this simulation, the effective component is supernova energy injection acting over a period of 10–30 Myr after initial

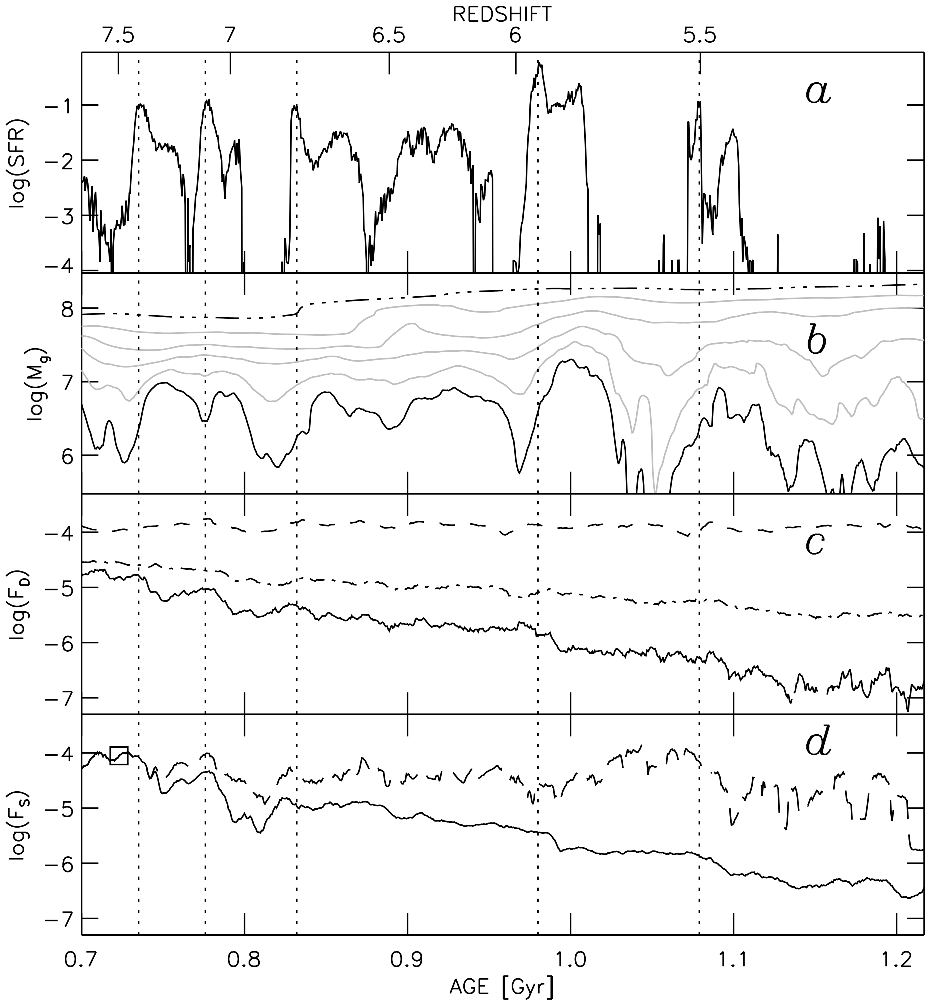


Figure 3.1: Star formation rate, variation of enclosed gas mass and variation of phase-space density for the collisionless components.

*a*) Star formation rate ($M_\odot\,yr^{-1}$) within a radius of 100 pc of the centre. Vertical dotted lines highlight 5 strong star formation peaks.

*b*) Enclosed gas mass ($M_\odot$) for various radii. The solid line is for a 100 pc radius, and the grey increase the radius by a factor of two each step. The triple-dot-dash line is the enclosed mass within 3.2 kpc.

*c*) The dark matter phase-space density ($M_\odot\,pc^{-3}\,km^{-3}\,s^3$) measured within 100 pc. The solid line indicates low velocity dark matter (see text) while the dash-dot is for all dark matter. The dashed line shows the behaviour in a simulation without stellar feedback.

*d*) The stellar phase-space density ($M_\odot\,pc^{-3}\,km^{-3}\,s^3$) measured within 100 pc. The solid line is for stars formed before $z = 7.5$ (time stamp denoted by the square), while the long-dash line is for all stars.

star formation. Thus, once initiated within a dense knot of gas, star formation rises to a peak and shuts down in around 10 Myr. The five highest peaks in the central star formation rate are marked with vertical dotted lines to guide the eye over the four panels of the figure.

The solid line in Figure 3.1b shows the enclosed gas mass in units of $M_\odot$ as a function of time within 100 pc. The enclosed gas mass shows the same cyclic behaviour as the star formation rate with a lag of 10–20 Myr. Gas falls into the inner regions, forming dense clouds and allowing star formation to begin. Stellar feedback starts to pressurize the gas leading to both compression and the driving of material out of the inner regions. The gas velocity dispersion varies from 10–$40\,\mathrm{km\,s^{-1}}$ within 100 pc, indicating crossing times of roughly 5–20 Myr. Thus the gas mass peaks slightly after the peak in star formation and then subsides.

The total gas mass (triple-dot-dash line in the same panel) within 3.2 kpc (the virial radius at $z = 8$) increases steadily due to fresh in-falling material, reaching $\sim 2 \times 10^8\,M_\odot$ at $z = 5$. Feedback associated with vigorous star formation can readily create hot gas (T $> 10^6$ K) and outflows exceeding the $100\,\mathrm{km\,s^{-1}}$ escape velocity. Such unbound gas can travel tens of kiloparsecs from the dwarf. However, the total mass in unbound (mostly hot) gas generated is comparable to the $3 \times 10^7\,M_\odot$ in stars created over the 500 Myr period shown in Figure 3.1. In-fall onto the galaxy continues steadily along cold filaments next to the outflow channels and is not disrupted by the outflow, as the figure indicates. The baryon fraction inside the virial radius is always moderately in excess of the universal baryon fraction. The gas mass within the star forming inner region fluctuates dramatically in response to feedback but much of this gas is simply cycling within the inner few hundred parsecs. Within 800 pc the gas content grows fairly smoothly as shown by the second-to-top grey curve.

The numerical values for star formation rates and mass outflows are a result of the specific sub-grid models and resolution used for this simulation (though the resolution is much higher than is typical). However, the qualitative picture is expected to be robust and is consistent with our understanding of feedback and its role in creating a bursty star formation history in smaller galaxies (Stinson et al., 2007). The gas within the entire halo is characterized by churning motions with colder gas moving in and hotter gas moving out. This is in contrast to the simple gas blow-out picture of the evolution of dwarf galaxies (e.g Navarro et al., 1996) where the entire star-forming gas content is at least temporarily evacuated. The advantage here is the continual availability of gas for ongoing star formation with bursts on the dynamical timescale of the dense inner regions (50–100 Myr) that repeatedly perturb the collisionless components. This type of churning also occurs in more massive galaxies (Brook et al., 2012).

Figure 3.1c shows the behaviour of the central dark matter phase-space density, approximated as $\rho/\sigma^3$, where $\rho$ is the mean dark matter density and $\sigma$ is the velocity dispersion within the central 100 pc. Whereas the fine-grained, dark matter, 6-dimensional phase-space density is strictly conserved, the coarse-grained dark matter phase-space density, which we are approximating with $\rho/\sigma^3$, is insensitive to adiabatic compression due to baryonic dissipation but should decrease monotonically due to irreversible (non-adiabatic) effects.

The dot-dash line is for all dark matter particles located within 100 pc of the centre at each simulation output. The solid line shows the behaviour of a group of dark matter particles with velocities less than $20\,\mathrm{km\,s^{-1}}$, selected at $z = 8$, and followed throughout the simulation. Both dark matter groups show a steady decrease in the coarse-grained phase-space density 10–20 Myr after a star formation peak. Note, however, that the low velocity dark matter exhibit much steeper gradients.

This decrease is associated with both an increase in their velocity dispersion and a decrease in their density. This persistent decrease of $\rho/\sigma^3$, unaffected by the gas returning to the core, demonstrates that the heating of collisonless matter through the gas-driven gravitational potential oscillations is irreversible. The long term effect is a random walk in orbital energy that redistributes dark matter particles into a cored profile of order 400 pc in size by $z = 5$ as shown by Mashchenko et al. (2008). In the same dwarf simulated without any star formation, the phase-space density remains relatively constant as shown by the dashed line.

## 3.3 Stars: The Other Collisionless Component

Stars also behave as a collisionless fluid, and so couple to the potential fluctuations created by stellar-feedback-driven gas motions. Indeed, the majority of stars are formed within the dwarf core and spread outwards by the end of the simulation. The central stellar density is regularly increased by new stars which are then dispersed to larger orbits. The long-dash line in Figure 3.1d shows the phase-space density for all stars within 100 pc. As the stellar density within this radius is replenished by star formation, there is no significant trend in the phase-space density. To examine the evolution of stars after their formation, we selected stars within the inner 100 pc that were formed before 0.72 Gyr and tracked their phase-space density over time as indicated by the solid line. The decrease in phase-space density is dramatic, comparable to that for the low-velocity-dispersion dark matter. Since the stars form from gas with velocity dispersion $\sim 20\,\mathrm{km\,s^{-1}}$, these trends reflect the greater efficiency of this heating mechanism for low velocity material. Note also that significant decreases in the phase-space density occur 10–20 Myr after the central bursts of star formation, as discussed above. In our simulated dwarf, stellar orbits are found to expand to beyond 1 kpc through the effects of this mechanism.

### 3.3.1 The Diffuse Spheroid

In this new picture, stars form preferentially in spatially concentrated star bursts near the gas-rich centres of small galaxies and then migrate to the outer parts of the galaxy. Orbital changes occur repeatedly for objects traversing the star forming core. This effect will not be limited to small galaxies but may become less pronounced for larger halos. The degree to which stars have migrated is a function of their time of formation and the period of time for which sufficiently vigorous potential fluctuations were available to pump their orbits. This provides an alternative to simply scaling the ELS view down to smaller halo masses.

Figure 3.2 shows that even though half the stars formed inside 100 pc (solid line), by the end of the simulation (500 Myr later) they fill the entire dwarf halo with no distinction between those that formed inside and outside 100 pc. New stars take time to move outward and when star formation stops, so does the orbital expansion. The result at $z = 5$ is a moderate trend to larger stellar ages with radius. This may explain the age and metallicity gradients believed to be present in the Local Group Dwarfs (Mateo, 1998).

### 3.3.2 Bound Star Clusters

As noted above, the star formation that occurs in the simulation is clustered in character due to the unusually high spatial resolution ($100\,\mathrm{M}_{\odot}$ per star particle) and modeling of low temperature cooling (Mashchenko et al., 2008), consistent with the majority of star formation in nature. The majority of these clusters are disrupted as the simulation progresses, and the stars are deposited across the stellar spheroid of

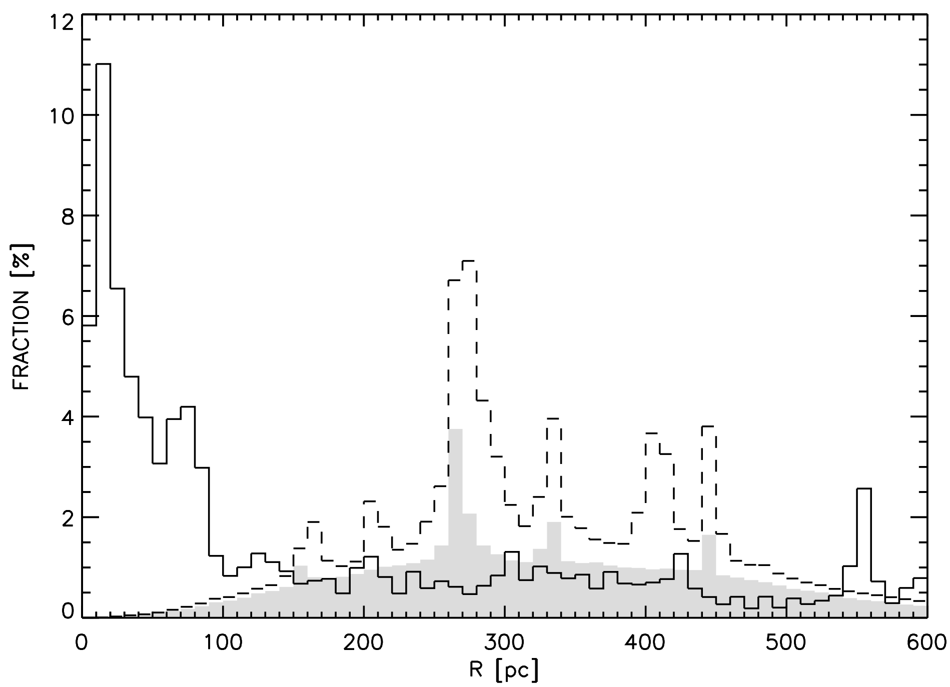


Figure 3.2: The normalized distribution of stellar formation radius (solid) and the final stellar radius (dashed). The shaded region corresponds to the distribution of final radii for the stars that formed within 100 pc.

the dwarf. This is partly a resolution effect as the gravitational resolution of the simulation (10 pc) will not result in smaller, more tightly bound clusters. There are, however, a few of these clusters that survived for at least 200 Myr. The four most massive and well resolved clusters (100–1000 stellar particles) were identified within the dwarf spheroid near the end of the simulation and their orbits traced backwards to the point at which 10% of the stars within each cluster had formed. The radial component of the orbits for the four clusters are shown in Figure 3.3. These four massive clusters form well within 100 pc but are then driven out to large radii as each pericentric passage brings them close to the actively star-forming galactic centre. The process is a random walk with an average tendency to increase the apocentric distance. These clusters also show changes in the direction and magnitude

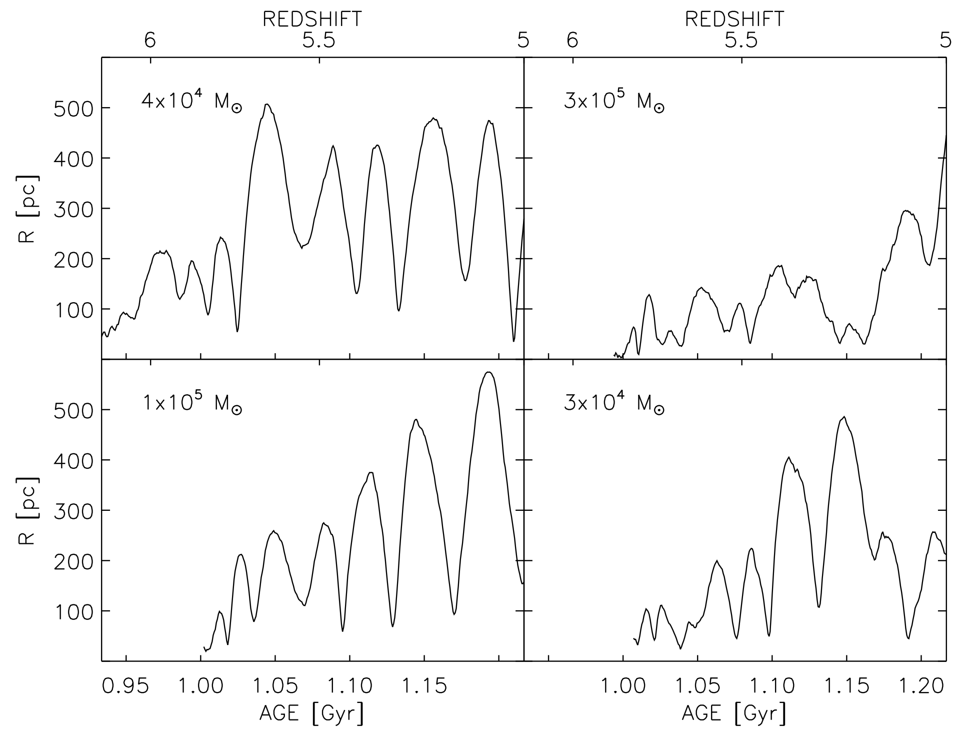


Figure 3.3: Evolution of orbital radii for four long-lived star clusters in the simulation.

of their orbital angular momenta. The process should be less effective for higher orbital velocities and is thus expected to saturate when the orbits are well outside the star forming region.

Our approach to the building of dwarf spheroids may shed light on the formation of Globular Clusters. Since the same mechanism migrates both stars and stellar clusters to the diffuse spheroid, it provides a natural explanation for the radial distribution seen in dwarf galaxies outside the Local Group (e.g. Miller, 2009). Furthermore, the time that the clusters are resident in the inner star forming region (which has grown to $\sim 300$ pc by $z = 5$) is typically at least $10^8$ yr. Visual inspection of the simulation indicates that dense gas knots move with the clusters during this period, thus providing a simple explanation for the recently observed multiple generations of stars within globular clusters (e.g D'Ercole et al., 2010).

## 3.4 Conclusions

We have presented a new framework for understanding the formation of the stellar spheroid in dwarf galaxies: All stars form in the nuclear regions and are then redistributed to eventually occupy the entire halo. The redistribution mechanism relies on strong fluctuations in the baryon-dominated central gravitational potential that are associated with stellar feedback as first demonstrated by Mashchenko et al. (2008). These fluctuations irreversibly affect the orbits and hence distributions of the collisionless components: dark matter, stars and star clusters. The key implications are:

• This process directly affects dwarf galaxies. In these galaxies a mild gradient with radius of increasing age and decreasing metallicity would be created as older stars achieve the largest orbits. Orbital redistribution stops when vigorous star formation ceases.

• The central density of stars stays fairly constant as new stars form to replace those migrating outwards.

• Globular cluster-like star clusters form in the ISM (and thus have no associated dark matter) and migrate outward over several orbital periods.

• The star clusters may form multiple generations of stars from enriched gas readily available in the nuclear regions. They will lose access to new gas as their orbits become larger.

• Continuous creation and outward migration of stars and globular clusters avoids the formation of a super-nucleus at the centre of most dwarf galaxies.

- Larger clusters become protected against tidal destruction as their orbits grow and the dwarf's dark-matter core becomes flattened.

- Mergers and tidal stripping will deposit these loosely bound stars and clusters into the halo of later generations of larger galaxies.

- Large star clusters formed in dwarf galaxies at high redshift, rather than in dark matter mini-halos, could be the primary source of Globular Clusters in all galaxies.

## Acknowledgements

This work has made use of the SHARCNET Consortium, part of the Compute/Calcul Cananda Network. AJM, HMPC and JWW are recipients of NSERC funding. HMPC achowledges support from CIfAR.

# Bibliography


Brook, C. B., Stinson, G., Gibson, B. K., et al. 2012, MNRAS, 419, 771

Bullock, J. S., & Johnston, K. V. 2005, ApJ, 635, 931

Bullock, J. S., Kolatt, T. S., Sigad, Y., et al. 2001, MNRAS, 321, 559

Burkert, A. 1995, ApJL, 447, L25

Carollo, D., Beers, T. C., Lee, Y. S., et al. 2007, Nature, 450, 1020

Carollo, D., Beers, T. C., Chiba, M., et al. 2010, ApJ, 712, 692

Côté, S., Carignan, C., & Freeman, K. C. 2000, AJ, 120, 3027

de Blok, W. J. G. 2010, AdAst, 2010

de Jong, J. T. A., Yanny, B., Rix, H.-W., et al. 2010, ApJ, 714, 663

De Lucia, G., & Helmi, A. 2008, MNRAS, 391, 14

Dekel, A., & Silk, J. 1986, ApJ, 303, 39

D'Ercole, A., D'Antona, F., Ventura, P., Vesperini, E., & McMillan, S. L. W. 2010, MNRAS, 407, 854

Dubinski, J., & Carlberg, R. G. 1991, ApJ, 378, 496

Eggen, O. J., Lynden-Bell, D., & Sandage, A. R. 1962, ApJ, 136, 748

Gilmore, G., Wilkinson, M. I., Wyse, R. F. G., et al. 2007, ApJ, 663, 948

Governato, F., Brook, C., Mayer, L., et al. 2010, Nature, 463, 203

Helmi, A. 2008, A&ARv, 15, 145

Klypin, A., Kravtsov, A. V., Bullock, J. S., & Primack, J. R. 2001, ApJ, 554, 903

Macciò, A. V., Stinson, G., Brook, C. B., et al. 2012, ApJL, 744, L9

Mashchenko, S., Couchman, H. M. P., & Wadsley, J. 2006, Nature, 442, 539

Mashchenko, S., Wadsley, J., & Couchman, H. M. P. 2008, Science, 319, 174

Mateo, M. L. 1998, ARA&A, 36, 435

McConnachie, A. W. 2012, AJ, 144, 4

Miller, B. W. 2009, Globular Clusters in Dwarf Galaxies, ed. Richtler, T. & Larsen, S., 141

Navarro, J. F., Eke, V. R., & Frenk, C. S. 1996, MNRAS, 283, L72

Navarro, J. F., Frenk, C. S., & White, S. D. M. 1995, MNRAS, 275, 720

Oh, S.-H., de Blok, W. J. G., Brinks, E., Walter, F., & Kennicutt, Jr., R. C. 2011, AJ, 141, 193

Pontzen, A., & Governato, F. 2012, MNRAS, 421, 3464

Robertson, B., Bullock, J. S., Font, A. S., Johnston, K. V., & Hernquist, L. 2005, ApJ, 632, 872

Searle, L., & Zinn, R. 1978, ApJ, 225, 357

Stadel, J., Potter, D., Moore, B., et al. 2009, MNRAS, 398, L21

Stinson, G. S., Dalcanton, J. J., Quinn, T., Kaufmann, T., & Wadsley, J. 2007, ApJ, 667, 170

Zinn, R. 1980, ApJ, 241, 602

Zolotov, A., Willman, B., Brooks, A. M., et al. 2010, ApJ, 721, 738

# Chapter 4

# The Celestial Buffet: multiple populations and globular cluster formation in dwarf galaxies

Reprinted from Aaron J. Maxwell, James Wadsley, H. M. P. Couchman, and Alison Sills *2014*, MONTHLY NOTICES OF THE ROYAL ASTRONOMICAL SOCIETY, *Volume 439, Issue 2, pp. 2043–2049, DOI: 10.1093/mnras/stu086. Published by Oxford University Press on behalf of the Royal Astronomical Society.* 

## 4.1 Introduction

Until recently, the standard picture of a globular cluster was that of a simple stellar population. It was thought that all the stars formed in one time, in one place, and from a single cloud with a uniform chemical abundance. However, high-precision photometry from the *Hubble Space Telescope* (e.g. Bedin et al., 2004; D'Antona et al., 2005; Piotto et al., 2005, 2007, 2012) revealed split main sequences and subgiant branches in many massive clusters, such as NGC 2808, M22, 47 Tuc, and NGC 1851. Simultaneously, high-resolution spectroscopic studies of globular cluster stars (e.g. Ramírez et al., 2001; Carretta et al., 2009a) showed that almost all globular clusters have no star-to-star variations in iron abundance. The variation in lighter elements, however, which had been characterized in bright giants for decades (e.g. Carretta & Gratton, 1994; Cohen, 1999; Gratton et al., 2006; Carretta et al., 2007b), was shown to extend down to stars on the main sequence (e.g. Gratton et al., 2001; Ramírez & Cohen, 2002; Carretta et al., 2003, 2004). Most surprisingly, a high He content is required to explain some of the observed properties of several of these clusters (e.g. Piotto et al., 2005; D'Antona et al., 2005; Carretta et al., 2007a; Piotto et al., 2012).

The ubiquity of this light element spread in all well-studied globular clusters (see the review by Gratton, Sneden, & Carretta, 2004) suggests globular clusters undergo a more complex formation process than that of a single burst of star formation. The chemical patterns, the split photometric sequences, and extended horizontal branches (e.g. Bedin et al., 2004) of globular clusters can be explained if, within the first few hundred million years of a cluster's existence, two or more populations of stars were formed (e.g. Ventura et al., 2001; D'Antona & Caloi, 2008). One was made from the same composition – which we will call pristine throughout this paper – as the stars of the halo: [Fe/H] $\simeq$ -2, and $\alpha$-enriched but otherwise having scaled-solar abundances of the light elements. The other generations were formed from material which has undergone hot hydrogen burning, occurring at temperatures above about $7 \times 10^7$ K. Burning hydrogen under these circumstances uses the Ne–Na and Al–Mg cycles (analogues to the lower temperature C–N–O cycle), and can produce He as well as the observed trends of the other light elements. The material which formed both populations, however, usually has the same Fe content.

The commonly accepted explanation for these abundances is a sequence of events that a nascent globular cluster must undergo (e.g. D'Antona & Caloi, 2008; Ventura & D'Antona, 2008a). First, the proto-globular cluster forms from pristine gas. After some time, the most massive stars explode as supernovae, but their ejecta have sufficient velocity to escape unhindered from the potential well of the cluster. Later, a population of *polluting* stars ejects their hot hydrogen-burnt material into the cluster at much lower velocities, so that the material is retained by the cluster. Shortly thereafter, the second population forms from a mixture of this material and additional pristine material that has fallen into the cluster, in order to reproduce the observed abundance variations (e.g. Carretta et al., 2009c; Ventura et al., 2013). These two populations then passively evolve to become the present-day cluster. This scenario broadly matches the observational constraints on the problem of multiple populations and extended horizontal branches in globulars, but there are two problems which we describe below.

The majority of recent papers currently favour asymptotic giant branch (AGB) stars as the polluters (e.g. Ventura & D'Antona, 2005b; D'Ercole et al., 2010) since the bottom of their convective envelopes can produce the required overabundance of Na and N versus O and C (e.g. Denisenkov & Denisenkova, 1989). However, the nucleo synthetic yields from AGB stars need to be carefully tuned (e.g. Denissenkov & Herwig, 2003; James et al., 2004), and there is still some uncertainty in the AGB evolution models (e.g. Ventura & D'Antona, 2005a, 2008b). Due to these problems, other polluters have been proposed: rapidly rotating massive stars (e.g. Decressin et al., 2007), massive binary stars (e.g. de Mink et al., 2009), and even stellar collisions (Sills & Glebbeek, 2010).

The second problem has to do with the mass budget for the polluted population, which can make up to 50 per cent of the present cluster mass (e.g. Carretta et al., 2009b; Piotto et al., 2012). If one assumes a normal initial mass function (IMF) and an initial cluster mass that is close to its present-day mass ($\sim 10^6\,M_\odot$), then the population of polluting stars can only produce at most a few percent of the cluster mass as material with which to form the polluted population (e.g. Cohen, Briley & Stetson, 2005). Most papers to date have addressed this issue by requiring the proto-cluster be at least 10 times more massive than the present cluster (e.g. D'Antona & Caloi, 2008; Ventura & D'Antona, 2008b; D'Ercole et al., 2010; Vesperini et al., 2013), added more enriched gas to the ejecta by flattening the AGB range of the IMF (e.g. D'Antona & Caloi, 2004; D'Antona et al., 2005), or both. Furthermore, highly unlikely star formation efficiencies of 100 per cent are required in the formation of the second population, or the mass-budget problem becomes even worse.

Bekki (2010, 2011) simulated the formation of a second generation of stars from AGB ejecta within a cluster. As expected (e.g. D'Antona & Caloi, 2004; D'Ercole et al., 2008), a second population formed soon after the first starburst, but with a spatial and kinematic distribution completely different from the first population. The simulations showed that the second population would be centrally condensed and show considerable rotation due to the dissipative processes required to drive the enriched material to realistic star-forming conditions. The initial cluster mass required to retain the AGB ejecta exceeded $6\times10^5\,M_\odot$, and even the best case scenario was only able to form $4\times10^4\,M_\odot$ in second population stars. Yet, an order of magnitude increase in initial stellar mass would only produce enough AGB ejecta to form the *present-day* mass of second generation stars. Self-enrichment thus requires the cluster to be tidally stripped on time-scales much shorter than their relaxation times (e.g. Vesperini et al., 2013), since the first generation stars would have distributions initially extending to larger radii.

The most straightforward solution to this problem was suggested by Bekki (2006): instead of treating the formation of globular clusters as simple stellar populations condensing from homogenous isolated gas clouds, they were treated as forming within the centres of dwarf galaxies at high redshift ($z \gtrsim 4$). This alleviated the mass budget problem, since now AGB ejecta from the surrounding dwarf galaxy spheroid would cool and settle to the centre, mix with the pristine material, and form the second population in the newly formed globular cluster. However, even this scenario failed to reproduce the observed trends (Bekki et al., 2007).

The problem is that the simple approach of Bekki (2006) would not make up the majority of globular clusters with variance only in the light elements. Bekki (2006) assumes the stellar nucleus of a dwarf progenitor is accreted on to a Milky Way (MW) sized halo, observable as a halo globular cluster. However, the likelihood that SNe ejecta will be retained by the dwarf increases as its halo mass grows, imposing a limit on how long the stellar nucleus can be considered uniform in abundance. This is evident in the broad range of Fe-enrichment exhibited by many of the Local Group Dwarfs, such as Fornax (e.g. Pont et al., 2004). Many globular clusters show very little dispersion in the Fe-peak elements (e.g. Ramírez et al., 2001; Carretta et al., 2009a), which suggests at least two possible constraints not discussed in Bekki (2006). Either all globular clusters formed in dwarf progenitors that were accreted by larger haloes extremely early, or some process halted star formation in the nucleus on long time-scales, preserving the uniform iron abundances.

There do exist peculiar globular clusters with dispersion in their heavy elements which would fit this model (Bekki & Norris, 2006). $\omega$ Cen is one example of a globular cluster with variations in [Fe/H] (e.g. Norris & Da Costa, 1995; Piotto et al., 2005), which can be explained if it is the remnant stellar nucleus of an accreted dwarf galaxy (e.g. Gnedin et al., 2002). Another is M54, located at the centre of the Sagittarius dwarf galaxy (Ibata, Gilmore & Irwin, 1995) and likely an example of $\omega$ Cen in an earlier accretion phase (Carretta et al., 2010). NGC 2419 has similarly been argued to be the core of a stripped dwarf galaxy (Mackey & van den Bergh, 2005; Cohen et al., 2010; Cohen, Huang & Kirby, 2011; Cohen & Kirby, 2012). Clearly, what is lacking in the Bekki (2006) model is a clear understanding of how the uniform heavy element abundance is preserved, if dwarf progenitors are the true sites of globular cluster formation.

In this paper, we provide a new framework in which we can understand the formation of all globular clusters that exhibit abundance variations. Like Bekki (2006), this new framework assumes the site of globular cluster formation is within the centres of dwarf galaxies. *Unlike* previous work, our framework proposes that these clusters are removed from the dwarf centres through dynamical evolution and end up on wide orbits, like those of the Fornax dwarf (e.g. Hodge, 1961; Mateo, 1998; Letarte et al., 2006), where they may be easily stripped. By proposing a physically motivated mechanism for globular cluster removal, our new framework provides a consistent solution to the problem of abundance spreads with the cluster and links the probability of a spread in [Fe/H] to the amount of time spent in the dwarf centre. We describe our new framework in §4.2, and provide an illustration of it in §4.3 using a highly resolved simulation of a dwarf galaxy at high redshift (Mashchenko, Wadsley & Couchman, 2008). We describe the setup in §4.3.1, with results in §4.3.2.

## 4.2 A New Framework For Forming Multiple Populations in Dwarf Galaxy Globular Clusters

The framework that will be outlined here rests on one key assumption: *all globular clusters exhibiting abundance spreads formed near the centre of high-redshift dwarf galaxy progenitors and were later accreted during the hierarchical build-up of present-day massive galaxy haloes*. As gas accretes on to the dwarf galaxy progenitor, it cools and collapses to the centre. Once the gas reaches sufficient densities ($\gtrsim 100\,\mathrm{m_H\,cm^{-3}}$) to form molecular clouds, star formation begins. This will lead to feedback from massive stars in the form of radiation, winds, and supernova explosions that suppress star formation for about 30 Myr. Massive amounts of gas will be swept out of the central regions, carrying the now $\alpha$-enriched material.

The feedback will cause significant gas mass re-distribution within the dwarf galaxy centre, in turn altering the central gravitational potential. Rapid fluctuations in the potential will lead to gravitational pumping of the collisionless components – dark matter (Mashchenko, Wadsley & Couchman, 2008; Governato et al., 2012; Pontzen & Governato, 2012) and stars (Maxwell et al., 2012; Teyssier et al., 2013). A globular cluster formed within the centre will be moved to larger and larger orbits with each star formation burst. The important point here is that even though the globular cluster is removed from the centre of the dwarf, *it will make multiple passages through the gas-rich centre*. On each pass, the globular cluster may accrete gas from the centre of the dwarf galaxy, including pollutants responsible for the light element abundance spread. However, it will also experience subsequent energy kicks, eventually placed on so large an orbit that further accretion will be halted.

Many groups have established through numerical experiments this energetic re-distribution of mass in dwarfs (e.g. Read & Gilmore, 2005; Mashchenko, Couchman & Wadsley, 2006; Mashchenko, Wadsley & Couchman, 2008; Governato et al., 2010, 2012; Pontzen & Governato, 2012). These studies focused on the transformation of the inner dark matter density profile from the cusps predicted by theory (e.g. Dubinski & Carlberg, 1991; Navarro, Frenk & White, 1995; Bullock et al., 2001; Klypin et al., 2001; Stadel et al., 2009) to the cores observed in Local Group dwarfs (e.g. Burkert, 1995; Côté, Carignan & Freeman, 2000; Gilmore et al., 2007; Oh et al., 2011). It has only been recently that attention has been paid to how this process would affect stars (Maxwell et al., 2012; Teyssier et al., 2013). Maxwell et al. (2012) focused on how this process would form spheroidal light profiles in the old stellar population, and by extension the presence of globular clusters at large projected radii from their hosts. In our framework, both the formation of dark matter cores and multiple population globular clusters are intimately linked through the same mechanism of mass re-distribution.

The centre of dwarf galaxies also contains a much deeper potential well than that of an isolated gas cloud or globular cluster. Assuming that AGB stars are in fact the polluters, their wind can be retained within the dwarf nuclei (e.g. Bekki & Norris, 2006) since the speed at which the wind travels from the stellar surface is about 40 $\mathrm{km\,s^{-1}}$ (e.g. Woitke, 2006). Supernovae can blow out gas at upwards of 500 $\mathrm{km\,s^{-1}}$ which can easily escape dwarf galaxies. Globular clusters have typical escape speeds (Harris, 1996; Gnedin et al., 2002) of 10–20 $\mathrm{km\,s^{-1}}$ and so would be unable to retain this hot gas. On the other hand, the AGB ejecta is retained in the deep potential and available for accretion (e.g. Conroy & Spergel, 2011) by globular clusters as they pass through the centre of the dwarf. The clusters do not need to begin with masses an order of magnitude greater than that presently observed to cause self-inflicted pollution (e.g. Cottrell & Da Costa, 1981); instead, they draw from a reservoir created by the surrounding stars, provided the gas is accreted efficiently.

Current models of the formation of the second population require some sort of dilution (e.g. Carretta et al., 2009c) of the polluted material with pristine gas in order to create the observed abundance anticorrelations. Since our framework places the formation site of the mixed abundance clusters within progenitor dwarf galaxies at high redshift, there should be plenty of gas in fall to lend itself to dilution (e.g. Maxwell et al., 2012). Eventually, the gas within the centre will become predominantly pristine and the cluster formation process can begin anew. A single dwarf galaxy could make several mixed abundance globular clusters within a few hundred Myr, long before Type Ia SNe begin to enrich the gas with Fe. This is in sharp contrast to the work of Bekki (2006) which would be more suitable for producing the more unusual objects that show clear [Fe/H] variations, such as $\omega$ Cen.

## 4.3 An Illustration

We use the cosmological simulation of a well resolved dwarf galaxy by Mashchenko, Wadsley & Couchman (2008) to demonstrate the salient points of our framework. This simulation has been extensively studied in the context of the cusp–core problem (for a recent review see de Blok, 2010) and the formation of Fornax-like spheroidal systems (Maxwell et al., 2012). The 12 pc force softening used in the simulation is comparable in scale to globular clusters and molecular clouds hosting star formation, but is still adequate for our purposes. Within the simulation, Maxwell et al. (2012) identified four bound star clusters over 100 times denser than the surrounding stellar spheroid that could be traced over 100 Myr.

However, the resolution was not high enough to resolve the internal structure of the clusters, and so we cannot measure dynamical properties such as their mass distribution or velocity dispersion. At these scales, accurate treatment of the formation of stars and the resultant feedback is required, which prevents us from directly studying the accretion of gas on to the cluster and the true mass of the clusters themselves. Since our framework applies to any collisionless component of matter, we need only use a suitable globular cluster tracer throughout the simulation to illustrate it in a cosmological context. Therefore, in the following setup, we use only the orbital properties of these clusters and treat the cluster mass as a free parameter.

### 4.3.1 Accretion

Since we cannot directly measure accretion on to a star cluster as it passes through the gas-rich centre of the dwarf, we use the first-order estimate of Bondi & Hoyle (1944):

$$\dot{M} \simeq 2\alpha\pi \frac{G^2 M^2}{(v_{\rm rel}^2 + c_{\rm s}^2)^{3/2}} \bar{\rho}, \tag{4.1}$$

where $M$ is the mass of the cluster, $\bar{\rho}$ is the ambient gas density, $v_{\rm rel}$ is the relative velocity between the cluster and the gas, and $c_{\rm s}$ is the sound speed of the gas. The numerical factor $\alpha$ lies between 1 and 2 for most cases (Bondi & Hoyle, 1944; Bondi, 1952), but we have assumed unity so that we may be conservative in our estimate of the accretion rate. Since we cannot directly measure the local gas density and temperature, we average the gas particle properties over a 35 pc sphere around the centre of mass of each cluster in each simulation snapshot. This is the typical tidal radius for the MW clusters (Harris, 1996) derived from the King surface density profiles (King, 1962, 1966), and similar to the maximum accretion radius derived from Equation (4.1) for a $10^6\,{\rm M}_\odot$ cluster and a sound speed of $10\,{\rm km\,s^{-1}}$.

To compute the bulk relative velocity, we use the mass-weighted relative velocity with respect to the centre of mass velocity of the cluster:

$$\vec{v}_{\text{rel}} = \frac{\sum m_i(\vec{v}_i - \vec{v}_{\text{com}})}{\sum m_i}, \tag{4.2}$$

for all gas particles within the 35 pc sphere whose temperature is below $1.5 \times 10^4$ K.

The original derivation of Equation (4.1) was for spherically symmetric accretion of a point mass moving through a uniform medium whose properties were measured very far from the point mass. Lin & Murray (2007) have shown that for extended mass distributions whether Equation (4.1) applies to the cluster as a whole, or to individual stars within the cluster, depends on the internal velocity distribution of the stars. Although we cannot directly measure the velocity distribution of the stars within the four clusters, the functional form of the accretion rate is preserved in both scenarios (Lin & Murray, 2007). Any uncertainty will be contained mainly in $\alpha$, which requires detailed numerical study (e.g. Naiman, Ramirez-Ruiz & Lin, 2011). Since each of the four clusters spends significant time with relative speeds of 20–30 km s$^{-1}$ with respect to the surrounding gas, and given the spherical symmetry of globular clusters, Equation (4.1) should give a good estimate of the amount of gas accreted by a globular cluster moving through regions of dense gas (Conroy & Spergel, 2011).

Once the gas has accreted on to the ‘surface’ of a globular cluster, it should disperse throughout the cluster on a very short time-scale. Using a mean half-mass radius of 4.3 pc (Harris, 1996) and a typical sound speed of 10 km s$^{-1}$ yields a crossing time of 0.4 Myr. This is significantly shorter than the cooling time for the accreted gas and the onset of star formation, which is expected to last 2–3 Myr (e.g. D’Ercole et al., 2008; Bekki, 2011), which is still shorter than the 10–20 Myr length of a typical accretion event experienced by the four clusters. Thus, once gas is accreted it will quickly condense to the centre of the cluster and begin to form stars.

#### 4.3.1.1 Pollution Source

We will assume that AGB stars are the source of the pollutants responsible for the light element abundance dispersion (e.g. Denisenkov & Denisenkova, 1989; D'Antona & Caloi, 2008), and that the winds from these stars distribute the pollutants. However, our framework is not tied to a specific polluter and so will be applicable regardless of whether AGB stars are the true culprit; all that we require is that the source is present within the dwarf galaxy. Most of the stars within the dwarf galaxy are found within 1 kpc (Maxwell et al., 2012) and the escape velocity from this radius is $60\,\mathrm{km\,s^{-1}}$, so we can safely assume that the AGB wind will stay bound to the galaxy.

Recently, Larsen, Strader & Brodie (2012) suggested that the star formation history of Fornax placed severe constraints on the AGB mass available. Although the simulation of Mashchenko, Wadsley & Couchman (2008) did not track the light element abundances of individual gas particles due to AGB feedback, we can verify that the star formation history of the dwarf galaxy would satisfy even the highest observed fraction of second generation — in other words, polluted — stars by mass. Since the star particles formed in the Mashchenko, Wadsley & Couchman (2008) simulation represent many stars, we must integrate over the IMF to obtain the fraction of each star particle that would be expected to contribute to enriching the surrounding gas. Given the uncertainties in AGB yields, we will focus only on the 3–6 $\mathrm{M_\odot}$ mass range (e.g. Ventura et al., 2001), although 6–8 $\mathrm{M_\odot}$ stars may also be a contributor (e.g. D'Ercole et al., 2012). Using a typical power-law index $\alpha = -2.3$ (Salpeter, 1955; Miller & Scalo, 1979; Kroupa, 2001; Chabrier, 2003) over the mass range 0.1–100 $M_\odot$, approximately 8 $M_\odot$ per 100 $M_\odot$ will undergo the AGB phase; increasing the upper limit to 8 $M_\odot$ would add roughly an extra 3 $M_\odot$ per 100 $M_\odot$. Assuming AGB stars lose at least 10 per cent of their initial mass over a period of 30–100 Myr yields a mean wind-loss rate of $10^{-2}$ $M_\odot$ hinspace $\mathrm{Myr}^{-1}$. Converting the star formation history of the dwarf into an AGB ejecta history yields over $10^5$ $M_\odot$ of pure AGB ejecta within 1 kpc over a few Myr.

In order to determine if this satisfies the observational constraints, we searched the literature (Ramírez & Cohen, 2002, 2003; Cohen & Meléndez, 2005; Cohen & Melendez, 2005; Carretta et al., 2006, 2007b,a,c, 2009c,b) for spectroscopic measurements of the Na–O anti correlation, and follow Carretta et al. (2009c) by splitting the stars into three components. We then used their simple dilution model to estimate that $\sim$7 per cent of the accreted mass needs to be composed of pure AGB ejecta in order to reproduce the global Na–O anticorrelation. In other words, a cluster whose final mass is $4 \times 10^6$ $M_\odot$ cluster with half of the stars showing signatures of enrichment would only require $1.5 \times 10^5$ $M_\odot$ of AGB ejecta. Furthermore, the diffusion time of the AGB ejecta through the inner 1 kpc of the dwarf galaxy is

$$t_{diff} \sim \frac{1\,\mathrm{kpc}}{v_{wind}} \simeq 24\,\mathrm{Myr}.$$

This suggests that there may be inhomogeneity in the amount of enrichment within the gas pool from which a cluster may accrete, further diversifying the amount of dispersion a given cluster will exhibit.

### 4.3.2 Results

In order to find the potential mass growth of the four clusters traced within the simulation, we numerically integrate Equation (4.1):

$$M(t) = \int_{t_o}^{t} \dot{M} \mathrm{d}t'. \tag{4.3}$$

We start the integration 30 Myr after the formation of each cluster since this represents the end of the SNe phase which will sweep out any residual gas from the formation of the initial stellar population. This allows sufficient time for the gas that formed the first generation cluster stars to be swept away by Type II supernovae. This is supported by the observation that the majority of the star formation within the simulation occurs in bursts separated by 50–100 Myr (Maxwell et al., 2012).

Since the mass growth is highly non-linear, we will represent it as the percentage increase in mass as a function of time:

$$\frac{M(t) - M(t_o)}{M(t_o)} \times \text{per cent}, \tag{4.4}$$

where $M(t_o)$ corresponds to the initial cluster mass. This is shown in Fig. 4.1, for three different initial masses: $5 \times 10^5$ M$_\odot$ as the solid line, $10^6$ M$_\odot$ as the short dashed line, and $2 \times 10^6$ M$_\odot$ as the long dashed line. The abscissa has been set to start at the formation time of each cluster. Each cluster experiences wildly different growth rates, despite living in the same dynamic halo.

First, the most massive clusters will accrete the most material at later times. It has been observed that the strength of the Na–O anticorrelation in globular clusters is correlated with the cluster mass (e.g. Recio-Blanco et al., 2006; Carretta et al., 2009b,a). Furthermore, the extent of the Na–O anticorrelation can be repro-

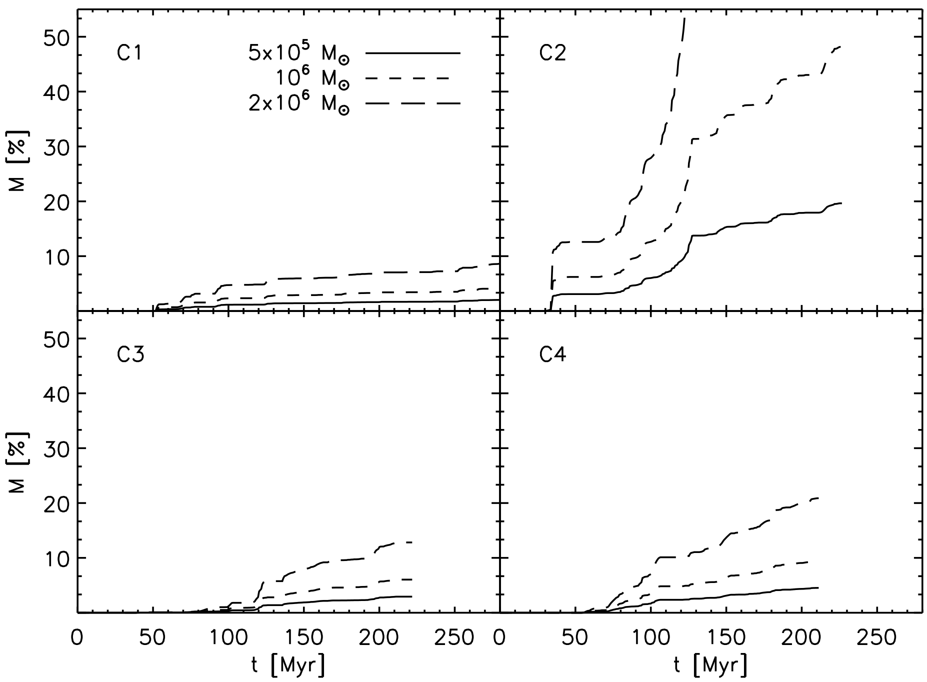


Figure 4.1: The percentage increase in mass estimated from Equation (4.1) as a function of time for the four clusters within the Mashchenko, Wadsley & Couchman (2008) simulation. The three lines represent the three different initial masses: $5 \times 10^5$ $M_\odot$ (solid), $10^6$ $M_\odot$ (short dashed), and $2 \times 10^6$ $M_\odot$ (long dashed). The fraction by which a cluster can increase its mass depends on the varying orbit, initial cluster mass, and gas density within the Bondi–Hoyle radius.

duced using a model wherein one source of material, either the pure AGB ejecta or the pristine gas, is diluted by the other. In other words, there exist two time-scales: one for the accumulation of pristine material, and one for the accumulation of AGB ejecta. Presumably, pristine material will accumulate at a rate dependent on the dwarf galaxy merger history, whereas the AGB ejecta will accumulate depending on the star formation history. If the most massive clusters can accrete more gas for a longer time during each pass through the centre, then our framework applied to the Mashchenko, Wadsley & Couchman (2008) simulation suggests that the pristine gas accumulates first, so that the more massive clusters can accumulate more

AGB ejecta later.

Secondly, the orbit of a cluster through its host dwarf progenitor primarily determines its mass growth. The orbits of the clusters, shown in grey in Fig. 4.2, grow with time due to the fluctuations in the gravitational potential induced by the re-distribution of the central dark matter mass. This is a purely stochastic process, since it depends on both the rate of gas accumulation in the dwarf progenitor centre, the star formation rate, and the supernovae rate. Each cluster will have a unique accretion history, even within the same dwarf galaxy progenitor, due to the varying number of AGB stars and their location within the dwarf, as well as the changing orbit. This is consistent with the observation that the amount of light element enrichment per MW globular cluster varies between 10 and 50 per cent by mass (e.g. Piotto et al., 2012).

Thus, we can consider the ratio of gas density to relative gas velocity as the accretion efficiency; a massive cluster passing quickly through a dense gas region may experience an accretion rate much lower than that of a lower mass cluster passing slowly through sparse pockets of gas. The mass increase experienced by a cluster is a discontinuous process: clusters experience 'growth spurts' as they pass through the centre of the dwarf galaxy progenitor where the densest gas is found. The split main sequences within the globular clusters (e.g. Piotto et al., 2012) would arise over time through the gradual combination of enriched and pristine material (e.g. Bedin et al., 2004; Piotto et al., 2005, 2007). The mass growth cannot continue indefinitely, however, as each boost in the cluster's orbit means that its relative velocity through the dwarf progenitor centre will increase, as shown in Fig. 4.2. The black lines show the accretion rate given by Equation (4.1) as a function of time for an initial mass of $2 \times 10^6$ $M_\odot$.

Increasing the relative velocity of a cluster through dense gas also increases

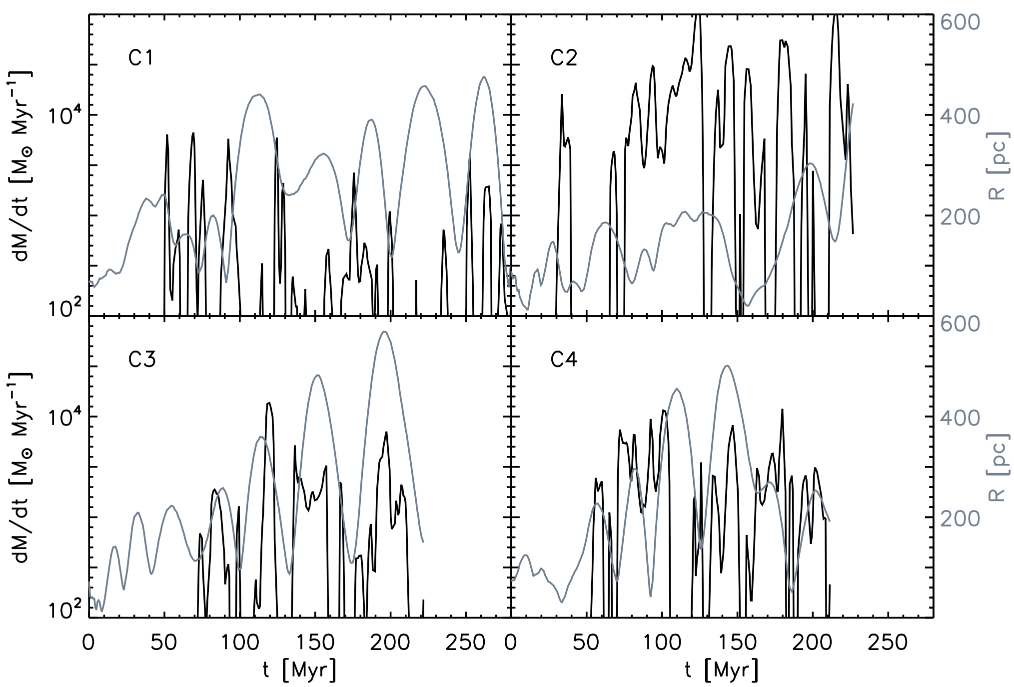


Figure 4.2: The accretion rate for each of the four clusters predicted from Equation (4.1) using an initial mass of $2\times10^6$ M$_\odot$, shown in black. We have applied a boxcar filter to the accretion rate to remove noise caused by the time-dependent sampling. We have also plotted the cluster orbital radius in grey.

the probability that the clusters may experience ram pressure stripping. Although Equation (4.1) does not take this into account, we can use the temporal behaviour of $v_{rel}$ of each cluster through the dense gas, shown in Fig. 4.3, to determine whether the accreted gas is susceptible to removal by hydrodynamic forces. Stripping will occur for globular clusters when the pressure of the accreted gas is less than the ram pressure of the ISM as it flows past the cluster. Ignoring the cooling and gravitational collapse of the accreted gas, this condition is satisfied when $v_{rel} \gtrsim v_{esc}$, the cluster escape velocity, for most situations (Mori & Burkert, 2000). In Fig. 4.3, this is represented by the three horizontal lines which correspond to the escape velocity from 10 pc for each of the cluster masses used in Fig. 4.1. It is clear that each

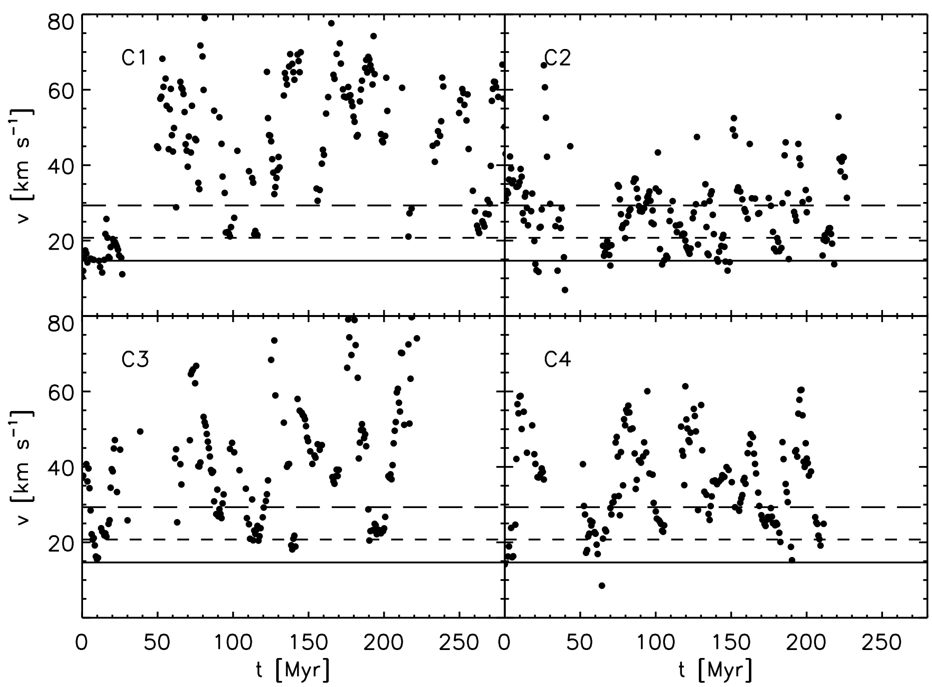


Figure 4.3: The filled circles represent the temporal behaviour of $v_{rel}$. The three solid lines represent escape velocities from 10 pc for each of the three cluster masses used in Fig. 4.1.

cluster spends a significant amount of time within 35 pc of gas with relative speeds of 20–30 km s$^{-1}$.

In general, the initial orbit of the cluster will significantly affect the ability for enriched gas to be accreted. The three clusters with the largest orbits would have accreted 10–20% of their initial mass, despite making multiple passes through the inner 100 pc of the dwarf galaxy progenitor. The cluster with the highest estimated mass growth accretes much of its material during the 100 Myr when its orbit is least eccentric. Finally, it experiences a huge energy boost that ejects the cluster past 300 pc, and were the simulation continued, it would probably experience a cut-off similar to that exhibited by the other three clusters.

## 4.4 Summary

We have proposed a new framework for the formation of multiple populations in dwarf galaxies. In this framework, the high-redshift progenitors of dwarf galaxies are the formation sites of globular clusters with light element abundance dispersions. The deeper potential well of the dwarf progenitors can easily retain the winds from AGB stars, thought to be the most likely source of the polluting material. Fluctuations in the gravitational potential, caused by the re-distribution of matter by star formation feedback ocurring at the centres of dwarf galaxies, will drive growth in the clusters orbit. In time, it will make multiple passes through the gas-rich dwarf centre, accreting a combination of pristine and polluted material.

We have examined this framework in the context of the first cosmological simulation of a highly resolved dwarf galaxy. Our results suggest that this framework broadly matches the mounting observational evidence of multiple populations in many, if not all, globular clusters. It suggests a timeline for enrichment that matches the dilution models used to explain the observed light element anticorrelations, such as that in Na–O, with the observation that more massive clusters have the largest abundance spreads. It also connects the stochastic nature of star formation and feedback to the observed spread in the number of second generation stars within each cluster, which is between 10 and 50 per cent by mass. Finally, it provides the clearest difference between our new framework and those previously proposed, since our framework provides the blueprint to form the whole population of globular clusters, not just those with heavy element abundance spreads. Thus, there exists at least two modes of stellar cluster formation within dwarf galaxies: the globular cluster channel and the stripped stellar nucleus channel.

## Acknowledgements

We thank our anonymous referee whose careful reading of this manuscript and insightful comments helped improve this paper. AJM, JW, HMPC, and AS are supported by NSERC. This work has made use of the SHARCNET Consortium, part of the Compute/Calcul Canada Network. This research has made use of NASA's Astrophysics Data System, and of the NASA/IPAC Extragalactic Database (NED) which is operated by the Jet Propulsion Laboratory, California Institute of Technology, under contract with the National Aeronautics and Space Administration. This research has made use of the VizieR catalogue access tool, CDS, Strasbourg, France.

# Bibliography


Bedin L. R., Piotto G., Anderson J., Cassisi S., King I. R., Momany Y., Carraro G., 2004, ApJL, 605, L125

Bekki K., 2006, MNRAS, 367, L24

Bekki K., 2010, ApJL, 724, L99

Bekki K., 2011, MNRAS, 412, 2241

Bekki K., Campbell S. W., Lattanzio J. C., Norris J. E., 2007, MNRAS, 377, 335

Bekki K., Norris J. E., 2006, ApJL, 637, L109

Bondi H., 1952, MNRAS, 112, 195

Bondi H., Hoyle F., 1944, MNRAS, 104, 273

Bullock J. S., Kolatt T. S., Sigad Y., Somerville R. S., Kravtsov A. V., Klypin A. A., Primack J. R., Dekel A., 2001, MNRAS, 321, 559

Burkert A., 1995, ApJL, 447, L25

Carretta E., Bragaglia A., Cacciari C., Rossetti E., 2003, A&A, 410, 143

Carretta E., Bragaglia A., Gratton R., D'Orazi V., Lucatello S., 2009a, A&A, 508, 695

Carretta E., Bragaglia A., Gratton R., Lucatello S., 2009b, A&A, 505, 139

Carretta E. et al., 2007a, A&A, 464, 939

Carretta E., Bragaglia A., Gratton R. G., Leone F., Recio-Blanco A., Lucatello S., 2006, A&A, 450, 523

Carretta E. et al., 2010, ApJL, 714, L7

Carretta E. et al., 2009c, A&A, 505, 117

Carretta E., Bragaglia A., Gratton R. G., Lucatello S., Momany Y., 2007b, A&A, 464, 927

Carretta E. et al., 2007c, A&A, 464, 967

Carretta E., Gratton R., 1994, Mem. Soc. Astron. Italiana, 65, 799

Carretta E., Gratton R. G., Bragaglia A., Bonifacio P., Pasquini L., 2004, A&A, 416, 925

Chabrier G., 2003, PASP, 115, 763

Cohen J. G., 1999, AJ, 117, 2434

Cohen J. G., Briley M. M., Stetson P. B., 2005, AJ, 130, 1177

Cohen J. G., Huang W., Kirby E. N., 2011, ApJ, 740, 60

Cohen J. G., Kirby E. N., 2012, ApJ, 760, 86

Cohen J. G., Kirby E. N., Simon J. D., Geha M., 2010, ApJ, 725, 288

Cohen J. G., Meléndez J., 2005, AJ, 129, 303

Cohen J. G., Melendez J., 2005, AJ, 129, 1607

Conroy C., Spergel D. N., 2011, ApJ, 726, 36

Côté S., Carignan C., Freeman K. C., 2000, AJ, 120, 3027

Cottrell P. L., Da Costa G. S., 1981, ApJL, 245, L79

D'Antona F., Bellazzini M., Caloi V., Pecci F. F., Galleti S., Rood R. T., 2005, ApJ, 631, 868

D'Antona F., Caloi V., 2004, ApJ, 611, 871

D'Antona F., Caloi V., 2008, MNRAS, 390, 693

de Blok W. J. G., 2010, AdAst, 2010

de Mink S. E., Pols O. R., Langer N., Izzard R. G., 2009, A&A, 507, L1

Decressin T., Meynet G., Charbonnel C., Prantzos N., Ekström S., 2007, A&A, 464, 1029

Denisenkov P. A., Denisenkova S. N., 1989, Astronomicheskij Tsirkulyar, 1538, 11

Denissenkov P. A., Herwig F., 2003, ApJL, 590, L99

D'Ercole A., D'Antona F., Carini R., Vesperini E., Ventura P., 2012, MNRAS, 423, 1521

D'Ercole A., D'Antona F., Ventura P., Vesperini E., McMillan S. L. W., 2010, MNRAS, 407, 854

D'Ercole A., Vesperini E., D'Antona F., McMillan S. L. W., Recchi S., 2008, MNRAS, 391, 825

Dubinski J., Carlberg R. G., 1991, ApJ, 378, 496

Gilmore G., Wilkinson M. I., Wyse R. F. G., Kleyna J. T., Koch A., Evans N. W., Grebel E. K., 2007, ApJ, 663, 948

Gnedin O. Y., Zhao H., Pringle J. E., Fall S. M., Livio M., Meylan G., 2002, ApJL, 568, L23

Governato F. et al., 2010, Nature, 463, 203

Governato F. et al., 2012, MNRAS, 422, 1231

Gratton R., Sneden C., Carretta E., 2004, ARA&A, 42, 385

Gratton R. G. et al., 2001, A&A, 369, 87

Gratton R. G., Lucatello S., Bragaglia A., Carretta E., Momany Y., Pancino E., Valenti E., 2006, A&A, 455, 271

Harris W. E., 1996, AJ, 112, 1487

Hodge P. W., 1961, AJ, 66, 83

Ibata R. A., Gilmore G., Irwin M. J., 1995, MNRAS, 277, 781

James G., François P., Bonifacio P., Carretta E., Gratton R. G., Spite F., 2004, A&A, 427, 825

King I., 1962, AJ, 67, 471

King I. R., 1966, AJ, 71, 64

Klypin A., Kravtsov A. V., Bullock J. S., Primack J. R., 2001, ApJ, 554, 903

Kroupa P., 2001, MNRAS, 322, 231

Larsen S. S., Strader J., Brodie J. P., 2012, A&A, 544, L14

Letarte B., Hill V., Jablonka P., Tolstoy E., François P., Meylan G., 2006, A&A, 453, 547

Lin D. N. C., Murray S. D., 2007, ApJ, 661, 779

Mackey A. D., van den Bergh S., 2005, MNRAS, 360, 631

Mashchenko S., Couchman H. M. P., Wadsley J., 2006, Nature, 442, 539

Mashchenko S., Wadsley J., Couchman H. M. P., 2008, Science, 319, 174

Mateo M. L., 1998, ARA&A, 36, 435

Maxwell A. J., Wadsley J., Couchman H. M. P., Mashchenko S., 2012, ApJL, 755, L35

Miller G. E., Scalo J. M., 1979, ApJS, 41, 513

Mori M., Burkert A., 2000, ApJ, 538, 559

Naiman J. P., Ramirez-Ruiz E., Lin D. N. C., 2011, ApJ, 735, 25

Navarro J. F., Frenk C. S., White S. D. M., 1995, MNRAS, 275, 720

Norris J. E., Da Costa G. S., 1995, ApJ, 447, 680

Oh S.-H., de Blok W. J. G., Brinks E., Walter F., Kennicutt, Jr. R. C., 2011, AJ, 141, 193

Piotto G. et al., 2007, ApJL, 661, L53

Piotto G. et al., 2012, ApJ, 760, 39

Piotto G. et al., 2005, ApJ, 621, 777

Pont F., Zinn R., Gallart C., Hardy E., Winnick R., 2004, AJ, 127, 840

Pontzen A., Governato F., 2012, MNRAS, 421, 3464

Ramírez S. V., Cohen J. G., 2002, AJ, 123, 3277

Ramírez S. V., Cohen J. G., 2003, AJ, 125, 224

Ramírez S. V., Cohen J. G., Buss J., Briley M. M., 2001, AJ, 122, 1429

Read J. I., Gilmore G., 2005, MNRAS, 356, 107

Recio-Blanco A., Aparicio A., Piotto G., de Angeli F., Djorgovski S. G., 2006, A&A, 452, 875

Salpeter E. E., 1955, ApJ, 121, 161

Sills A., Glebbeek E., 2010, MNRAS, 407, 277

Stadel J., Potter D., Moore B., Diemand J., Madau P., Zemp M., Kuhlen M., Quilis V., 2009, MNRAS, 398, L21

Teyssier R., Pontzen A., Dubois Y., Read J. I., 2013, MNRAS, 429, 3068

Ventura P., D'Antona F., 2005a, A&A, 439, 1075

Ventura P., D'Antona F., 2005b, ApJL, 635, L149

Ventura P., D'Antona F., 2008a, MNRAS, 385, 2034

Ventura P., D'Antona F., 2008b, A&A, 479, 805

Ventura P., D'Antona F., Mazzitelli I., Gratton R., 2001, ApJL, 550, L65

Ventura P., Di Criscienzo M., Carini R., D'Antona F., 2013, MNRAS, 431, 3642

Vesperini E., McMillan S. L. W., D'Antona F., D'Ercole A., 2013, MNRAS, 429, 1913

Woitke P., 2006, A&A, 452, 537

Chapter 5

# Conclusions

The three preceding chapters within this thesis span a broad range of topics in galactic astrophysics. Stellar populations, the formation of globular clusters, the energy budget for cusp destruction, element anomalies in globular clusters, star formation feedback: all are areas of active research interest but rarely cross. In this chapter I will describe how these chapters advance our understanding of these areas and tie them together into a cohesive framework for further research. This thesis began with a simple idea: if the simulation of Mashchenko et al. (2008) is a believable demonstration of the formation of a density core in an initially cuspy dark matter halo, then how would the dynamical evolution of the stellar component be affected? Both stars and dark matter particles are collisionless, and the core formation paradigm of Mashchenko et al. (2006) utilizes this feature to drive collisionless matter out of the centre of the halo. It must also be pointed out that this thesis at no point rules out more exotic theories, such as warm dark matter or self-interactions, for the formation of cores in dark matter halos. Rather, it challenges these theories by describing how baryons reshaping dark matter halos simultaneously explains other astrophysical phenomena.

The intent of Chapter 2 was to counter the main argument from Peñarrubia et al. (2012) that the cumulative star formation history expected in $\Lambda$CDM theory was incompatible with the presence of dark matter cores in dwarf galaxy halos. More specifically, Peñarrubia et al. argued that the cumulative supernova feedback energy of the average dwarf galaxy could only produce dark matter cores if it was converted entirely into dark matter orbital energy. By imposing a more physically motivated boundary condition than that employed by Peñarrubia et al., the new calculations presented in Chapter 2 showed that the energy required to form cores from an initially cuspy halo is relatively low. Supernovae alone can form dark matter cores with no additional sources of feedback energy or modifications to the current dark matter particle model. Consequently, any dwarf galaxy that experiences localized star formation within dense gas near the bottom of the galactic potential should form a dark matter core.

Chapter 2 also defined, for the first time, a measure of the core radius that is completely independent of the assumed dark matter density profile. This was motivated by the difficulty of comparing the core radius estimates from different works that, historically, have used the scale radius as the core radius. Instead, this new core radius is defined by the slope of the density profile. If observations fail to map the rotation profile far enough to resolve the outer slope of the density profile, it is difficult to constrain the scale radius which must be matched to the rollover in density. Since our new definition is defined directly from measurable quantities derived from the rotation profile (e.g. $M$ and $\rho$) it can be tightly constrained, even with limited data.

The new energy difference between cusped and cored halos, $\Delta E$, calculated in Chapter 2 can be traced to the choice of $r_{\rm m}$, the radius at which both halos are indistinguishable in terms of radial density *and* total mass. A physical argument for normalizing both halos to a small fraction of the halo radius can be made: the efficiency with which stellar feedback energy is transferred to dark matter depends on how significantly stars and gas contribute to the local gravitational potential. Naturally, this will be in the centres of dark matter halos where the gas has condensed to high enough densities to undergo star formation. This is an important distinction between the work of Chapter 2 and that of Peñarrubia et al. (2012), because it leads one to conclude that it is the distribution of dark matter within the centre of the halo that sets the energy budget, and *not the large scale halo properties* as previously assumed.

The constraint that the radius where the two halos match be 2–3 times the core radius was motivated by numerical experiment. Although dark matter cores have been formed in both particle and grid hydrodynamic simulations (e.g. Mashchenko et al., 2008; Teyssier et al., 2013; Madau et al., 2014), many of the simulations have been done with the GASOLINE hydrodynamics code (Wadsley et al., 2004) using a similar supernova feedback recipe (Stinson et al., 2006; Shen et al., 2013). It remains for future work to determine whether the given ratio between the core and match radii is a robust prediction of the dark matter core formation process. A key question is how the parameter $\epsilon_{\rm SN}$, the fraction of energy from each type II supernova injected into the surrounding gas, determines $\epsilon$, the ratio of $\Delta$E to the cumulative supernova energy available (as determined by the total stellar mass of the dwarf galaxy). It was shown in Chapter 2 that when averaged over the cumulative star formation history:

$$\epsilon = \int \epsilon(t)\,\mathrm{dt},$$

for dwarf galaxies such as Fornax the core formation process is extremely inefficient; as little as 0.1 per cent of the total feedback energy is required to make up the energy difference between the pre- and post-core halo.

What determines $\epsilon(t)$, the time-dependent injection of stellar feedback energy into the dark matter, is still unknown, but it is clear that factors such as the halo mass, gas density, star formation rate, and the merger history of the halo will be of influence. Future exploration of $\epsilon(t)$ will require a combination of both cosmological and idealized dark matter simulations. Idealized simulations are required since cosmological simulations make it difficult to determine the properties (both central and large scale) of a given dark matter halo due to merger processes; tuneable parameters, such as $\epsilon_{\rm SN}$, also require controlled study. It is also of interest to study the dark matter core formation process with the many new numerical schemes approximating physical phenomena that have been incorporated into GASOLINE over the past decade. Prescriptions for the ultra-violet background from the reionisation of the universe (e.g. Haardt & Madau, 1996; Madau et al., 2004; Madau & Haardt, 2009; Haardt & Madau, 2012), the formation of molecular hydrogen (e.g. Christensen et al., 2012), entropy mixing of gas (e.g. Shen et al., 2010) and improvements to the unresolved supernova-driven bubble phase (e.g. Keller et al., 2014) were not in the original Mashchenko et al. (2008) simulation.

It is also unclear how the process of core formation in dark matter halos actually works. Mashchenko et al. (2006) described a process in which the bulk gas motions induced by star formation feedback acted as a resonant driver, swishing back and forth through the halo centre 'kicking' dark matter particles before being ejected from the centre; Mashchenko et al. (2008) showed that dense gas knots were indeed present in the centre of the simulated dwarf. Pontzen & Governato (2012) characterized it in terms of an impulsive blowout — characteristic of the arguments put forward by Navarro et al. (1996) and Read & Gilmore (2005) — but on a much smaller scale in terms of the total mass ejected from the galactic centre. Both models, however, emphasize the periodic bulk motions that are synonymous with 'bursty' star formation — peaks and troughs in the star formation rate representative of the interplay between dense gas condensing to form stars and supernova feedback blowing the dense gas away. Future study of these intricate details of the core formation process is necessary, both in terms of numerical simulations and analytic descriptions.

If only the central properties of the dark matter halo control the formation of a core, as Chapter 2 suggests, then we can begin to understand certain global properties of dark matter cores across all galactic morphology and environments. In $\Lambda$CDM, the properties of both galaxies and dark matter halos are dependent on the hierarchical formation history. Dark matter sub-halos accreted onto the primary halo will have their edges stripped by tidal forces as they sink deeper into the global gravitational well, while gas is stripped from the galaxy as it feels the ram pressure of the hot halo. These processes will significantly affect the global properties of a dwarf galaxy as a function of environment, but are less likely to affect the central properties of halos that host dwarf galaxies.

The fact that dark matter cores are observed in dwarf galaxies independent of their environment is a logical conclusion of the work presented in Chapter 2. Figure 2.5, where I have shown for the first time a prediction of core radius as a function of stellar mass — as opposed to previous studies which focused on the halo mass — is a reflection of this new focus on central properties. Recent cosmological simulations of cored dwarf galaxies by Shen et al. (2013) show similar relations between stellar mass and dark matter core radius (Madau et al., 2014). It must be stressed that in this discussion, where we focus largely on dwarfs, the total stellar mass of the galaxy can be considered a *central* property of the halo. A key result of Chapter 3 is that a significant fraction of the star formation in a dwarf galaxy at high redshift is within a few hundred parsecs of the centre. This is consistent with the fact that many dwarf galaxies contain their total stellar mass within roughly 500–1000 pc (Mateo, 1998; McConnachie, 2012).

Chapter 3 expands on these results by studying how the stellar population would be affected as a dark matter core forms within the halo. In fact, it is more appropriate to consider how collisionless particles — both stars and dark matter — evolve as the central gravitational potential is perturbed. If this process does not discriminate between stars and dark matter as expected, then their density profiles should be similar. Thus, the presence of a dark matter core should signal the presence of a stellar core. Furthermore, the stellar radius of the dwarf galaxy should be commensurate with the dark matter core radius[1] since the central stars should migrate out of the centre. Although Chapter 3 used the simulation of Mashchenko et al. (2008) to demonstrate that both the central stellar and dark matter particle orbits evolve similarly, it has been verified by subsequent simulations (e.g. Governato et al., 2014). The combined results of Chapters 2 and 3 are a significant contribution to our understanding of the formation of dark matter cores and the dwarf galaxies which are hosted within them.

Since $\Delta E$ depends sensitively on $r_{\mathrm{m}}$, which the first two chapters of this thesis argue is much less than the halo radius, and the concentration of the halo (which also sets the total mass within $r_{\mathrm{m}}$, see Chapter 2) we can begin to understand certain stellar properties of dwarf galaxies. Small dark matter cores (of order a few hundred pc) can be formed relatively quickly — the Mashchenko et al. (2008)

[1]Or, more precisely, with the halo match radius if the previous correlation between the core and match radius holds.

simulation showed a sizable core forming within roughly 100 Myr — without having to invoke high star formation rates. The rapidity of this process also prevents strongly cusped stellar density distributions (termed stellar nuclei), despite the fact that most of the star formation is within 200 pc in the Mashchenko et al. (2008) simulations. If this process continues unabated, it would naturally explain the stellar age and metallicity gradients found within the Local Group dwarf galaxies; these gradients, along with the presence of dark matter cores and the absence of stellar nuclei in dwarf galaxies, are synonymous with central cyclic star formation.

Since initially small cores will form quickly, it is expected that most cored dark matter halos will survive the hierarchical merger process. The phase space evolution of a merger between two collisionless halos will preserve the steepest cusp after relaxation (Dehnen, 2005); however, the relatively low values of $\Delta E$ — and thus the rapid formation rate of a dark matter core — suggest that many of the low mass dark matter halos are cored relatively early. Even the accretion of a dark matter cusp will not prevent the formation of a dark matter core so long as cyclic star formation can occur post merger and drive bulk gas motions significant enough to perturb the gravitational potential. Although Chapters 2 and 3 have presented a global overview of the process of core formation, by studying the dark matter cores and detailed star formation histories of individual dwarf galaxies it should be possible to constrain $\epsilon$. Unfortunately, there is currently no comprehensive study of the central slopes of dark matter halos due to the difficulty in measuring them from stellar kinematic data (e.g. Walker & Peñarrubia, 2011, and references therein).

An attractive alternative for constraining $\epsilon$ can be developed directly from Chapter 3. A large number of early type galaxies from the Fornax and Virgo Clusters Surveys (Côté et al., 2004; Jordán et al., 2007) have had their surface brightness profiles mapped (e.g. Ferrarese et al., 2006; Côté et al., 2007). Glass et al. (2011)

showed that distribution of the inner slopes of the *stellar* density profiles for these galaxies exhibit a continuous spread from flat to cusped ($0 < \gamma_* < 1$), and a subsequent study by Turner et al. (2012) quantified the 'strength' of the stellar nucleus in the dwarfs. If the properties of the central stellar and dark matter densities are indeed connected, as argued in Chapter 3, then observations of stellar kinematics within these galaxies (e.g. Toloba et al., 2011; Ryś et al., 2013; Toloba et al., 2014) should be able to verify this. Not only would stellar brightness profiles become a powerful tool for probing the structure of dark matter halos in dwarf galaxies where kinematic data are unavailable, but, more importantly, they could be used to set powerful constraints on the nature of the core formation process in dark matter halos. Whereas the proposed core formation paradigm of Mashchenko et al. (2006) explains the connection between stellar and dark matter density as due to their collisionless nature, it is unclear whether warm dark matter or other core formation theories make similar predictions.

Aside from differentiating between the various solutions to the core-cusp problem, determining what sets $\epsilon$ for a given dwarf galaxy would further progress our understanding of the formation of dark matter cores. First, it would help clarify how the growth of the core is limited, given that Chapter 2 suggests the growth of the core is unbounded. There may be a preferred shape and depth to the gravitational potential — determined by the properties of the whole halo (see Chapter 2) — that allows the most energy to be transferred from the supernova-driven bulk motions of the gas to the collisionless particles. Quenching of star formation or gas accretion might also inhibit core growth.

We can thus conclude from Chapters 2 and 3 that the central stellar and dark matter densities can easily be reduced given the average present day stellar mass in dwarf galaxies. Forming cores in dark matter halos is a possible solution to the

*Too Big to Fail* problem (Boylan-Kolchin et al., 2011) since cored densities have reduced rotation profiles compared to the cuspy halos predicted in dark-matter-only simulations (e.g. Zolotov et al., 2012; Brooks & Zolotov, 2014). Reducing the efficiency of star formation in simulated dwarfs which should not prevent dark matter cores from forming given the modest energy requirements, contrary to the arguments of Boylan-Kolchin et al. (2012). The corresponding dark matter density decrease ($\rho_c/\rho_o$) when transitioning from the cusp to a core is typically 2–5 times, relieving the inherent mismatch between dwarf galaxy luminosity and central mass densities. A similar decrease should be present in the stellar density as well, producing low surface brightness dwarf galaxies along with cored dark matter halos.

Another key result of Chapter 3 is the realization that stellar clusters might survive the chaotic churning of the dense gas within the centre of the dwarf galaxy, as seen in the Mashchenko et al. (2008) simulation. The massive amount of high density gas that will collect in the centre will naturally lead to clustered star formation, which in turn will provide the energy necessary to drive the perturbations in the gravitational potential. If these simulated clusters are the precursors to present-day globular clusters, it would explain why dwarf galaxies host globular clusters on large orbits; rather than forming at the edges of the dwarf, their orbits were driven there. Fornax, unlike many of the other Local Group dwarf galaxies, hosts five globular clusters (Hodge, 1961). The same process that places these globular clusters on such large orbits also aids their survival. Any massive body moving through a density distribution will undergo dynamical friction: the gravitational wake creates an over-density behind the massive particle, resulting in gravitational deceleration. Dynamical friction thus depends on the mass of the body, the local mass density, and the relative velocity between the two. If Fornax hosted a dark matter cusp, a massive globular cluster would be expected to spiral into the centre of the galaxy in a short 1–2 Gyr, but a cored density distribution considerably lengthens the time it takes for the cluster to sink (Goerdt et al., 2006).

Although Fornax is the exception and not the rule for Local Group dwarfs when it comes to hosting globular clusters, many of the dwarf galaxies surveyed in the Fornax and Virgo clusters possess globular clusters as well (e.g. Peng et al., 2008). Future work is needed in order to determine what factors affect the formation of globular clusters within dwarfs and their orbital evolution. Stellar mass may be a factor; Fornax's stellar mass is 10–100 times larger than many of the dwarfs of the Local Group but 10–100 times less massive than many of the dwarfs in the Virgo and Fornax galaxy clusters. If we consider the estimates of $\Delta E$ from Chapter 2, a global average value of $\epsilon$ sets the minimum stellar mass required to form a core in a given dark matter halo. Conversely, collisionless dark matter halos (and by extension, stars) can contract to higher densities adiabatically if an increase in gas density significantly deepens the central gravitational potential (e.g. Sellwood, 2003; Dubinski et al., 2009). The bulk motions driven in the gas by star formation feedback may become ineffective if the halo mass grows.

Establishing where these upper and lower stellar mass bounds exist, and under what conditions a core may or may not form, will shed light on how the diverse range of stellar light profiles, dark matter core sizes, and globular cluster counts arise in dwarf galaxies. Inhibiting the growth of a dark matter core may lead to cuspy stellar brightness profiles by preventing the recently formed stars from leaving the centre, or decrease the time required for star clusters to spiral into the centre; this would explain the parallels found between globular cluster and compact dwarf galaxy light profiles (Haşegan et al., 2005). The accretion of dense dark matter halos or star clusters would also lead to cuspy profiles across all stellar mass ranges. The significant ultraviolet flux required to reionize the universe may also inhibit the ability for dense star forming regions to form at the centres of dwarf galaxies.

The typical dwarf galaxy dark matter halo is between $10^9$–$10^{10}$ $M_\odot$, which corresponds to a virial temperature of 4000–22000 K and virial speeds of 10–30 km $s^{-1}$. The background UV flux responsible for the reionisation of the universe will heat the cold dense gas within these dwarf galaxies to similar temperatures. Thus, it is expected (and verified by cosmological simulations) that UV reionisation would suppress dense central star formation in dwarf galaxies. Self-shielding by atoms and molecules in dense clouds could alleviate this problem. The ability for a globular cluster to form might be inhibited by the efficiency with which a molecular cloud self shields. A prescription for self-shielding by atomic and molecular gas has been implemented in the hydrodynamics code GASOLINE (Wadsley et al., 2004), but it is resolution dependent (Christensen et al., 2012).

A simple way to estimate self-shielding of molecular hydrogen gas has been provided by Draine & Bertoldi (1996) and is used both in the Christensen et al. (2012) implementation as well as others (e.g. Gnedin et al., 2009). It requires a physically accurate estimate of the column density between the molecular cloud and all radiation sources. In GASOLINE, this is proxied by the product of the density and resolution element of a gas particle. Unfortunately, this leads to systematically low column densities if both the resolution length and gas particle mass are smaller than the typical size scale and mass of a typical cloud. An ad hoc solution would be to impose a minimum length scale defined by the size of molecular clouds. However, an improved method for estimating the column density is currently being implemented in GASOLINE (R. M. Woods et. al., *in prep*.). It should then be possible to study how the large scale properties of star forming regions affect the ability for a core to form, especially in dense galactic environments.

The large sample of dwarf galaxies from the Local Group and the Fornax and Virgo galaxy clusters emphasizes diversity in many galaxy properties. One cannot, however, discount the various gravitational interactions in these high density environments that can significantly alter the dynamic properties of matter, both luminous and dark, within these galaxies. There have been a number of Low Surface Brightness (LSB) galaxies identified within 50 Mpc, and they are largely isolated from other galaxies. Like many of the dwarf galaxies in the Local Group, they are hosted within cored dark matter halos; unlike most dwarf galaxies, they exhibit signs of current star formation. These LSBs may represent a new tool for studying the core formation process free of many of the complications that arise in high density environs[2].

Chapter 4 of this thesis represents an extension of the solution to the core-cusp problem to a seemingly unconnected problem found in the Milky Way globular clusters. If globular clusters are not the archetypal simple stellar population, forming in one place at the same time with the same initial elemental abundances, then the dynamic centre of high redshift dwarf galaxies may be their true site of formation. Since star clusters are expected to gain orbital energy from stellar feedback, they will naturally make multiple passes through the centre of the dwarf galaxy. It is expected that ejecta from the old stars within the dwarf galaxy and accreted gas from the surrounding cosmic web will continuously collect and mix in the centre; the stellar clusters would theoretically be able to accrete enough of this material to form a second generation of stars. Chapter 4 shows that this is plausible given simulations which exhibit dark matter core formation. Furthermore, the accretion would be discontinuous and eventually quenched as the relative velocity between the cluster and the surrounding gas grows. These facets of the model are consis-

[2] To that end, I have been on two (albeit unsuccessful) proposals — one to the Canada-France-Hawaii Telescope (Proposal ID 14AC014) and one to the Hubble Space Telescope (Cycle 22, Proposal ID 815) — to detect globular clusters in these galaxies and study their global properties.

tent with the current observations of multiple populations in Globular Clusters: the spread in both ages and abundances suggest the second population formed in distinct bursts very shortly after the first generation. Finally, these anomalous clusters are driven to the edges of their host dwarf galaxies where they can then be easily accreted onto the stellar halos of more massive galaxies.

Although Chapter 4 is an attractive model for the formation of multiple populations, more work will be required to validate the theory. A more quantitative study will determine whether the efficiency by which stellar clusters accrete material on each pass through the centre of the dwarf galaxy, and the fraction of the accreted material that actually forms stars, can viably satisfy these observational constraints. Recent studies of the sodium-oxygen anti-correlation in globular clusters (e.g. Carretta et al., 2014) still show the significant spread discussed in Chapter 4. It is becoming increasingly evident that this is most likely due to spectroscopic errors as photometric data consistently depicts well defined gaps in globular cluster main sequences (e.g. Milone et al., 2014).

Dwarf galaxies represent the building blocks of larger galaxies in the $\Lambda$CDM cosmological model. As such, their dynamical evolution has a significant impact on our understanding of present-day galaxies. This thesis represents a cohesive study of how many of the peculiar stellar properties evident in dwarf galaxies are tied to the formation (or lack thereof) of a constant density core within the host dark matter halos.

# Bibliography

Boylan-Kolchin, M., Bullock, J. S., & Kaplinghat, M. 2011, MNRAS, 415, L40

—. 2012, MNRAS, 422, 1203

Brooks, A. M., & Zolotov, A. 2014, ApJ, 786, 87

Carretta, E., Bragaglia, A., Gratton, R. G., et al. 2014, A&A, 564, A60

Christensen, C., Quinn, T., Governato, F., et al. 2012, MNRAS, 425, 3058

Côté, P., Blakeslee, J. P., Ferrarese, L., et al. 2004, ApJS, 153, 223

Côté, P., Ferrarese, L., Jordán, A., et al. 2007, ApJ, 671, 1456

Dehnen, W. 2005, MNRAS, 360, 892

Draine, B. T., & Bertoldi, F. 1996, ApJ, 468, 269

Dubinski, J., Berentzen, I., & Shlosman, I. 2009, ApJ, 697, 293

Ferrarese, L., Côté, P., Jordán, A., et al. 2006, ApJS, 164, 334

Glass, L., Ferrarese, L., Côté, P., et al. 2011, ApJ, 726, 31

Gnedin, N. Y., Tassis, K., & Kravtsov, A. V. 2009, ApJ, 697, 55

Goerdt, T., Moore, B., Read, J. I., Stadel, J., & Zemp, M. 2006, MNRAS, 368, 1073

Governato, F., Weisz, D., Pontzen, A., et al. 2014, arXiv:1407.0022

Haardt, F., & Madau, P. 1996, ApJ, 461, 20

—. 2012, ApJ, 746, 125

Haşegan, M., Jordán, A., Côté, P., et al. 2005, ApJ, 627, 203

Hodge, P. W. 1961, AJ, 66, 83

Jordán, A., Blakeslee, J. P., Côté, P., et al. 2007, ApJS, 169, 213

Keller, B. W., Wadsley, J., Benincasa, S. M., & Couchman, H. M. P. 2014, MNRAS, 442, 3013

Madau, P., & Haardt, F. 2009, ApJL, 693, L100

Madau, P., Rees, M. J., Volonteri, M., Haardt, F., & Oh, S. P. 2004, ApJ, 604, 484

Madau, P., Shen, S., & Governato, F. 2014, ApJL, 789, L17

Mashchenko, S., Couchman, H. M. P., & Wadsley, J. 2006, Nature, 442, 539

Mashchenko, S., Wadsley, J., & Couchman, H. M. P. 2008, Science, 319, 174

Mateo, M. L. 1998, ARA&A, 36, 435

McConnachie, A. W. 2012, AJ, 144, 4

Milone, A. P., Marino, A. F., Bedin, L. R., et al. 2014, MNRAS, 439, 1588

Navarro, J. F., Eke, V. R., & Frenk, C. S. 1996, MNRAS, 283, L72

Peñarrubia, J., Pontzen, A., Walker, M. G., & Koposov, S. E. 2012, ApJL, 759, L42

Peng, E. W., Jordán, A., Côté, P., et al. 2008, ApJ, 681, 197

Pontzen, A., & Governato, F. 2012, MNRAS, 421, 3464

Read, J. I., & Gilmore, G. 2005, MNRAS, 356, 107

Ryś, A., Falcón-Barroso, J., & van de Ven, G. 2013, MNRAS, 428, 2980

Sellwood, J. A. 2003, ApJ, 587, 638

Shen, S., Madau, P., Conroy, C., Governato, F., & Mayer, L. 2013, arXiv:1308.4131

Shen, S., Wadsley, J., & Stinson, G. 2010, MNRAS, 407, 1581

Stinson, G., Seth, A., Katz, N., et al. 2006, MNRAS, 373, 1074

Teyssier, R., Pontzen, A., Dubois, Y., & Read, J. I. 2013, MNRAS, 429, 3068

Toloba, E., Boselli, A., Cenarro, A. J., et al. 2011, A&A, 526, A114

Toloba, E., Guhathakurta, P., van de Ven, G., et al. 2014, ApJ, 783, 120

Turner, M. L., Côté, P., Ferrarese, L., et al. 2012, ApJS, 203, 5

Wadsley, J. W., Stadel, J., & Quinn, T. 2004, NewA, 9, 137

Walker, M. G., & Peñarrubia, J. 2011, ApJ, 742, 20

Zolotov, A., Brooks, A. M., Willman, B., et al. 2012, ApJ, 761, 71